

NO POST-PROCESSING
RETURN TO LIBRARY
DEPT. 022

A Semi-Direct Solver for Compressible Three-Dimensional Rotational Flow

Chung Chang and John J. Adamczyk
Lewis Research Center
Cleveland, Ohio

May 1983

NASA



LM180612E

904329
M84-10461

1
NASA-TR-83314
COPY ON MICROFICHE
N83-34908

TABLE OF CONTENTS

SUMMARY.	Page 1
INTRODUCTION	1
I – GOVERNING EQUATIONS.	3
I.1 – Munk-Prim Flows	3
I.1.1. – Vector Form.	3
I.1.2. – Tensor Form.	6
I.2 – Incompressible Flows.	7
II – SOLUTION STRATEGY	7
II.1 – Munk-Prim Substitution Principle and Its Application	7
II.2 – Outer Loop	9
II.3 – Inner Iteration Loop	10
III – APPLICATIONS TO A SHEAR FLOW IN A TURNING CHANNEL.	16
III.1 – Problem Definition and Solution Procedure	16
III.2 – Numerical Results	19
CONCLUSIONS.	22
APPENDIX A – Basic Theorems of the Outer Loop.	23
APPENDIX B – Inlet Flow Conditions, Outflow Conditions, and Boundary Conditions	28
APPENDIX C – Inner Loop Stability Analysis	31
REFERENCES	34

A SEMI-DIRECT SOLVER FOR COMPRESSIBLE THREE-DIMENSIONAL ROTATIONAL FLOW

Sin-Chung Chang and John J. Adamczyk

National Aeronautics and Space Administration
Lewis Research Center
Cleveland, Ohio

SUMMARY

An iterative procedure is presented for solving steady inviscid 3-D subsonic rotational flow problems. The procedure combines concepts from classical secondary flow theory with an extension to 3-D of a novel semi-direct Cauchy-Riemann solver. It is developed for generalized coordinates and can be exercised using standard finite difference procedures. The stability criterion of the iterative procedure is discussed along with its ability to capture the evolution of inviscid secondary flow in a turning channel.

INTRODUCTION

Quite often in fluid flows, one observes a complex cyclic flow pattern on planes normal to the primary flow direction. This flow structure is often referred to as "secondary flow." It is attributed to the streamwise component of vorticity that is generated by the deflection of the primary shear flow due to a boundary surface. Thus the primary driving force behind this phenomenon is the centrifugal pressure gradient in the main flow. The role of viscosity is of secondary importance. Practical examples of hardware in which one finds such flows are turbomachinery blade rows, transition diffuser ducting and fan-jet exhaust mixers. It is well known that the prediction and control of secondary flow within these devices can lead to a substantial increase in their aerodynamic performance.

One of the first theoretical efforts at describing the generation of secondary flow was by Squire and Winter (ref. 1). This paper described the generation of secondary flows in a turning channel, with the fluid assumed to be inviscid. Later Hawthorne (refs. 2 and 3) extended the analysis of Squire and Winter to arbitrary inviscid shear flow. This was then followed by the work of Lakshminarayana and Horlack (ref. 4) in which the effects of viscosity were included. These works provided the theoretical basis of our understanding of secondary flow phenomena. Unfortunately, except for the case of small entry shear or small flow deflection, these analyses do not provide a solution procedure for general secondary flows. Researchers interested in calculating secondary flows have either attempted to numerically solve the governing equations derived by these authors or numerically solve an equivalent reduced form of the Navier-Stokes equation (refs. 5 to 7). The present work lies midway between these two extremes. It combines some of the theoretical concepts suggested by the work of Hawthorne with the numerical methods suggested by the work of Martin (ref. 8).

The governing differential equations which are iteratively solved in this paper describe a steady, compressible, inviscid and non-heat-conducting fluid flow in the absence of external body forces. These equations can effectively model many features of secondary flows (refs. 9 and 10). The compressible fluid is assumed to obey the perfect gas equation of state and have constant

specific heat capacities. We will refer to the class of flows which are governed by the above equations as Munk-Prim flows to acknowledge the applicability of the Munk-Prim substitution principle (ref. 11) which significantly simplifies their solution. The details of this substitution principle and its application to the current problem are fully discussed in Section II. Briefly, it entails mapping an arbitrary Munk-Prim flow into a substitute flow which is either homentropic (i.e., uniform entropy) or homenergetic (i.e., uniform total enthalpy). The choice of substitute flow is made by specifying a scalar α (referred to as the Munk-Prim gauge factor) which remains constant along the flow streamlines. A properly chosen substitute flow, as will be shown later, can be solved with less computational effort. Upon obtaining the substitute flow solution, the solution to the original problem is constructed by a mapping procedure. Under this mapping procedure, the pressure field, Mach number and streamline pattern of the substitute flow are identical to those of the original flow.

The current solution procedure can also be applied to incompressible flows which satisfy continuity and the inviscid momentum equations, since the solution procedure follows directly the procedures used to construct the solution to homentropic compressible flows.

The implementation of the Munk-Prim flow solver is presented on the flow chart shown in figure 1. The procedure is iterative and consists of two interacting loops. The derivation of the equations solved in each loop is presented in Section I. In the outer loop, the total pressure, total temperature and vorticity distributions are found for a given velocity field. The solution strategy is presented in Section II and the questions of initial conditions and uniqueness of solution are addressed in Appendix A. An interesting feature of the current solution procedure for the vorticity vector is that it sidesteps solving the coupled 3-D vorticity transport equation (ref. 12). Rather the vorticity vector is formed from the solutions of two uncoupled partial differential equations (PDE's).

In the inner loop, the velocity and mass density fields are updated so as to satisfy the continuity equation and the condition that the curl of the velocity equals the vorticity. Within this loop, the total pressure, total temperature and vorticity distributions are assumed known. The iteration procedure by which the velocity and mass density fields are updated is also presented in Section II. This scheme is a 3-D extension of Martin's semi-direct procedure for solving the general 2-D Cauchy-Riemann problem (ref. 8). The boundary conditions associated with it are discussed in Appendix B while its convergence criterion is discussed in Appendix C.

The results of several subsonic flow computations are presented in Section III to illustrate the development of secondary flow in a turning channel. For weak secondary flows at low Mach numbers, the computed results are shown to be in excellent agreement with the theoretical prediction of Squire and Winter. For large secondary flows two cases were analyzed, the first being the generation of secondary flow due to inlet velocity shear, the second being the generation of secondary flow due to inlet temperature shear. Both cases resulted in the generation of significant nonlinear effects which caused the flow pattern to take on a turbulent-like structure. Finally, to demonstrate the usefulness of the Munk-Prim substitution principle, each Munk-Prim problem was solved twice, i.e., by employing a homentropic and then a homenergetic substitute flow mapping. Both procedures are shown to give identical results to within truncation error.

I - GOVERNING EQUATIONS

(I.1) Munk-Prim Flows

(I.1.1) Vector Form

The differential equations of the present analysis are the
Continuity equation

$$\vec{\nabla} \cdot (\rho \vec{V}) = 0 \quad (I.1)$$

Momentum equation

$$(\vec{V} \cdot \vec{\nabla})\vec{V} + \frac{1}{\rho} \vec{\nabla} P = 0 \quad (I.2)$$

and Entropy equation

$$\vec{V} \cdot \vec{\nabla} S = 0 \quad (I.3)$$

where \vec{V} , ρ , P , and S are the velocity vector, mass density, static pressure, and specific entropy, respectively. The above equations can be recast in terms of total pressure P_0 , total temperature T_0 , and velocity \vec{V} by employing the following thermodynamic relationships:

$$\rho = \frac{P_0}{RT_0} \left(1 - \frac{\vec{V} \cdot \vec{V}}{2 C_p T_0} \right)^{\frac{1}{\gamma-1}} \quad (I.4)$$

$$P = P_0 \left(1 - \frac{\vec{V} \cdot \vec{V}}{2 C_p T_0} \right)^{\frac{\gamma}{\gamma-1}} \quad (I.5)$$

and

$$S = C_p \ln T_0 - R \ln P_0 \quad (I.6)$$

Here C_p is the specific heat capacity at constant pressure, R the ideal gas constant, and γ the ratio of specific heat capacities. The parameters C_p , R , and γ are all constants for Munk-Prim flows. Throughout this study, the focus is to find the five independent variables P_0 , T_0 , and \vec{V} which satisfy the five independent equations (eqs. (I.1) to (I.3)). All other variables are considered functions of these fundamental variables.

To simplify the solution of the numerical problem, equations (I.1) to (I-6) are nondimensionalized by scaling length, pressure, temperature and density against a reference length L^* , a reference pressure P^* , a reference temperature T^* , and a reference density ρ^* (P^* , T^* , and ρ^* are assumed to satisfy the perfect gas law). Any additional reference variable is formed directly from P^* , T^* , and ρ^* . (For example, the dimensionless velocity $\vec{V} \stackrel{\text{def.}}{=} \frac{\vec{V}}{\sqrt{P^*/\rho^*}}$ and the dimensionless entropy $\frac{(S - S^*)}{R}$ with $S^* \stackrel{\text{def.}}{=} C_p \ln T^* - R \ln P^*$.) This results in a set of dimensionless flow equations which retain their original form with a dimensionless gas constant $R = 1$ and a dimensionless heat capacity $C_p = \frac{\gamma}{(\gamma - 1)}$.

In the remainder of this subsection, we will collect the differential equations which are used in the two iteration loops which form the solver. To proceed, one notes that equation (I.2) and the thermodynamic relations can be combined to form Crocco's equation, i.e.

$$\vec{V} \times \vec{\Omega} = \vec{\nabla} h_0 - T \vec{\nabla} S \quad (\text{I.7})$$

Here h_0 and T are the specific total enthalpy and absolute flow temperature, respectively. The vorticity vector $\vec{\Omega}$ is defined as

$$\vec{\Omega} = \vec{\nabla} \times \vec{V} \quad (\text{I.8})$$

and since $\vec{\nabla} \cdot (\vec{\nabla} \times \vec{A}) = 0$ where \vec{A} is an arbitrary differentiable vector field, the vorticity field must be solenoidal, i.e.,

$$\vec{\nabla} \cdot \vec{\Omega} = 0 \quad (\text{I.9})$$

In the current analysis Crocco's equation is used in place of the momentum equation. Also, since $\vec{\nabla} \cdot \vec{V} \times \vec{\Omega} = 0$, equations (I.3) and (I.7) imply that

$$\vec{V} \cdot \vec{\nabla} h_0 = 0 \quad (\text{I.10})$$

i.e., the specific total enthalpy is conserved along a streamline. With the aid of equation (I.6) and the relation:

$$h_0 = C_p T_0 \quad (\text{I.11})$$

Equations (I.3) and (I.10) can be replaced with the equivalent expressions:

$$\vec{V} \cdot \vec{\nabla} P_0 = 0 \quad (\text{I.12})$$

and

$$\vec{V} \cdot \vec{\nabla} T_0 = 0 \quad (I.13)$$

In the inner iteration loop, P_0 , T_0 , and $\vec{\Omega}$ are provided by the outer loop and the objective is to find a density ρ and a velocity \vec{V} which satisfy equations (I.1) and (I.8). The details of the inner loop iteration procedure are provided in Section II.

In the outer loop, the velocity field \vec{V} is assumed known and the objective is to find a total pressure P_0 , a total temperature T_0 , and a vorticity $\vec{\Omega}$ which satisfy equations (I.7), (I.9), (I.12), and (I.13). The evaluation of these variables can be divided into three steps. First, the unknowns P_0 and T_0 are solved using equations (I.12) and (I.13). This can be done if the inlet profiles of P_0 and T_0 are known. In the second step, the variables h_0 , T and S which appear on the right side of equation (I.7) are evaluated from the updated P_0 and T_0 field. In the final step, the vorticity vector $\vec{\Omega}$, which is required to satisfy equations (I.7) and (I.9), is constructed according to Theorem 2 of Appendix A. The result is

$$\vec{\Omega} = \vec{\nabla} h_0 \times \vec{\nabla} \tau + \vec{\nabla} S \times \vec{\nabla} \mu \quad (I.14)$$

where the two scalar functions τ and μ satisfy the equations

$$\vec{V} \cdot \vec{\nabla} \tau = 1 \quad (I.15)$$

and

$$\vec{V} \cdot \vec{\nabla} \mu = -T \quad (I-16)$$

(In deriving eqs. (I.14) to (I-16), it was assumed that $\vec{V} \neq 0$ and either $\vec{\nabla} h_0 \neq 0$ or $\vec{\nabla} S \neq 0$ within the solution domain.) The motivation for expressing $\vec{\Omega}$ in the form of equation (I.14) is that it can be obtained directly from the solution of two uncoupled first order PDE's. This procedure is far simpler than trying to solve equations (I.7) and (I.9) directly. The solution of equations (I.15) and (I.16) requires as input the inlet profile of τ and μ . These profiles, according to Theorem 1 of Appendix A, must be chosen to be consistent with the streamwise vorticity at the inlet.

In the present analysis, the substitute flows are either homentropic ($\vec{\nabla} S = 0$) or homenergetic ($\vec{\nabla} h_0 = 0$). For homentropic flows, the second term on the right side of equation (I.14) vanishes. As a result, there is no need to solve equation (I.16). Furthermore, for this class of flows, T_0 becomes a function of P_0 (see eq. (II.5)) which eliminates the need to solve equation (I.13). Thus only two PDE's, i.e., equations (I.12) and (I.15) need to be solved in the outer loop for homentropic flows. Similarly, for homenergetic flows, only equations (I.12) and (I.16) need to be solved. This observation

justifies our earlier contention that the use of the Munk-Prim substitution principle can lead to a relatively simple procedure for solving the general Munk-Prim problem.

(I.1.2) Tensor Form

In the previous subsection, the basic equations for the two iteration loops were derived using vector notation. Before these equations are solved in a non-Cartesian computational space, they shall be converted to general tensor forms. If we adopt Einstein's summation convention (which we shall use throughout this paper), then in terms of the general computational coordinates $\{x^i\}$, the tensor forms of the outer loop equations (I.12) to (I.16) are, respectively,

$$V^i \frac{\partial P_0}{\partial x^i} = 0 \quad (I.17)$$

$$V^i \frac{\partial T_0}{\partial x^i} = 0 \quad (I.18)$$

$$\sqrt{g} \, \Omega^i = \epsilon^{ijk} \left(\frac{\partial h_0}{\partial x^j} \frac{\partial \tau}{\partial x^k} + \frac{\partial S}{\partial x^j} \frac{\partial \mu}{\partial x^k} \right) \quad (I.19)$$

$$V^i \frac{\partial \tau}{\partial x^i} = 1 \quad (I.20)$$

and

$$V^i \frac{\partial \mu}{\partial x^i} = -T \quad (I.21)$$

In the above equations V^i is the contravariant velocity vector, Ω^i is the contravariant vorticity vector, g is the determinant of the covariant metric tensor g_{ij} , and ϵ^{ijk} is the contravariant Levi-Civita tensor density. It should be understood that the range of tensor indices, unless otherwise noted, is 1, 2, 3.

The tensor forms of the inner loop equations (eqs. (I.1) and (I.8)) are, respectively,

$$\frac{\partial F^i}{\partial x^i} = 0 \quad (I.22)$$

and

$$\sqrt{g} \Omega^i = \epsilon^{ijk} \frac{\partial V_k}{\partial x^j} \quad (I.23)$$

where F^i is the contravariant mass flux vector density defined as

$$F^i \stackrel{\text{def.}}{=} \rho \sqrt{g} g^{ij} V_j \quad (I.24)$$

The variables which appear in equations (I.23) and (I.24) and were not defined previously are V_i , the covariant velocity vector and g^{ij} the contravariant metric tensor.

(I.2) Incompressible Flows

The analysis of the previous subsection can be extended to incompressible flows. For these flows, the governing equations are equations (I.1), (I.2), and

$$\rho = \text{constant} \quad (I.25)$$

These equations can be nondimensionalized by introducing a reference length

L^* , a reference density $\rho^* \stackrel{\text{def.}}{=} \text{fluid density}$, a reference velocity V^* and a reference pressure $p^* \stackrel{\text{def.}}{=} \rho^* (V^*)^2$. This results in a set of dimensionless flow equations which retain their original form with a dimensionless density of $\rho = 1$.

Combining equations (I.2), (I.8), and (I.25) yields

$$\vec{V} \times \vec{\Omega} = \vec{\nabla}(P_0/\rho) \quad (I.26)$$

with

$$P_0 \stackrel{\text{def.}}{=} p + \left(\frac{1}{2}\right) \rho V^2 = \text{total pressure} \quad (I.27)$$

As a result of equations (I.25) and (I.26), equation (I.12) is also valid for this special class of flows.

Equations (I.1), (I.8), (I.9), (I.12), and (I.26) are the equations to be solved for incompressible flows. Their solution can be obtained in a fashion similar to that for the homentropic flows.

II - SOLUTION STRATEGY

II.1 Munk-Prim Substitution Principle and Its Application

In Section I, it was shown that a Munk-Prim flow can be specified in terms of total pressure P_0 , total temperature T_0 and the velocity vector \vec{V} . The

Munk-Prim substitution principle states that, if P_0 , T_0 , and \tilde{V} specify a given Munk-Prim flow, then one can generate another Munk-Prim flow (referred to as the substitute flow) by the following transformation:

$$P'_0 = P_0, T'_0 = T_0/\alpha^2, \tilde{V}' = \tilde{V}/\alpha \quad (II.1)$$

where P'_0 , T'_0 and \tilde{V}' are the flow variables of substitute flow and α (Munk-Prim gauge factor) satisfies the equation:

$$\tilde{V} \cdot \tilde{v}_\alpha = \tilde{V}' \cdot \tilde{v}_\alpha = 0 \quad (II.2)$$

The proof of this principle follows directly from equations (I.1) to (I.6). From equation (I.5) and equation (II.1), it is seen that the static pressure is invariant under a Munk-Prim transformation. Similarly, the Mach number and the streamline pattern are also invariant under this transformation.

The substitution principle associated with Munk-Prim flows can be used to reduce the computational effort required to solve the general Munk-Prim flow problem. This reduction in effort is made possible by a proper choice of α . To explore this further, let α be equal to

$$\alpha = \alpha_1 \stackrel{\text{def.}}{=} \sqrt{T_0} P_0^{\frac{1-\gamma}{2\gamma}} \quad (II.3)$$

or

$$\alpha = \alpha_2 \stackrel{\text{def.}}{=} \sqrt{T_0} \quad (II.4)$$

Both α_1 and α_2 satisfy equation (II.2) since T_0 and P_0 are constants along a streamline. If $\alpha = \alpha_1$, then equations (II.1) and (II.3) coupled with equation (I.6) imply that

$$S' = 0 \quad \text{and} \quad T'_0 = P'_0 \frac{\gamma-1}{\gamma} = P_0 \frac{\gamma-1}{\gamma} \quad (II.5)$$

i.e., the substitution flow is homentropic. Similarly, if $\alpha = \alpha_2$,

$$T'_0 = 1 \quad \text{and} \quad P'_0 = P_0 \quad (II.6)$$

i.e., the substitute flow is homenergetic. Solutions with either $S' = 0$ or $T'_0 = 1$ require less work to evaluate since their generation requires two

fewer equations to be solved per outer iteration cycle than that for the general flow problem.

The inlet conditions of a substitute flow can be evaluated from those of the original flow with the aid of equations (II.1), (II.3), and (II.4). Using these conditions and the solid wall boundary conditions (these conditions are invariant under the Munk-Prim transformation) along with a specified outflow condition, a substitute flow solution can be computed.

To generate the solution to the original problem from the solution of the substitute flow problem, the Munk-Prim gauge factor $\alpha_1(\alpha_2)$ must be evaluated throughout the flow field. This is accomplished by integrating equation (II.2). With $\alpha_1, (\alpha_2)$ known, the solution to the original problem is found by employing equation (II.1).

II.2 Outer Loop

In Section I, it was shown that only equations (I.17) and (I.20) or equations (I.17) and (I.21) need to be solved in the outer loop if a solution to a substitute flow problem is desired. These PDE's are first order and linear if the velocity field is assumed known. They may be solved using a standard marching procedure for hyperbolic equations. The algorithm used to integrate these equations in the present study was constructed based on the work of Hartree (ref. 13). It will be explained using equation (I.20) as an example. We assume that the computational domain is a parallelepiped which is bounded by four solid walls in x^2 and x^3 directions (see fig. 2(a)). We further assume that V^1 is positive everywhere and that all the values of τ are known on the grid plane GP1.

For an interior grid point A on GP2 at which t is to be evaluated, a point Q' on GP1 is found (see fig. 2(b)) such that the vector $\overrightarrow{Q'A}$ is in the direction of the known velocity vector at A (denoted by $V^i(A)$). The velocity vector at Q' (denoted by $V^i(Q')$) is computed by linearly interpolating (four point bivariate interpolation (ref. 14)) the velocity vectors at the four surrounding grid points A', B', C' and D'. The average of $V^i(Q')$ and $V^i(A)$ is then evaluated and set equal to $\tilde{V}^i(A)$. Next a point Q is located on GP1 such that the vector \overrightarrow{QA} points in the direction of $\tilde{V}^i(A)$. The value of τ at point Q (denoted by $\tau(Q)$) is then found by linear interpolation using the known value of τ at A', B', C', and D'. In the final step, τ is evaluated at point A (denoted by $\tau(A)$) from the equation

$$\tau(A) = \tau(Q) + \frac{\delta x^1}{\tilde{V}^1(A)} \quad (II.7)$$

where δx^1 is the distance between GP1 and GP2. If point A is a boundary grid point, the above procedure becomes two-dimensional (the normal velocity component vanishes at the channel walls). The integration of the three remaining transport equations (eqs. (I.17), (I.18), and (I.21)) can be performed in a similar fashion.

Once the transport equations are solved, the vorticity field is updated according to equation (I.19). The finite difference form of this equation is obtained by approximating grad with a second order central difference operator. The only exception occurs at the boundary where the normal derivative which appears in grad is approximated by either a forward or backward second order difference operator.

II.3 Inner Iteration Loop

The basic equations which are solved in the inner loop were identified in the previous section. They are equations (I.22), (I.23), and (I.24) and are repeated here for clarity,

$$\frac{\partial F^i}{\partial x^i} = 0 \quad (II.8)$$

$$\sqrt{g} \Omega^i = \epsilon^{ijk} \frac{\partial V_k}{\partial x^j} \quad (II.9)$$

$$F^i = \rho \sqrt{g} g^{ij} V_j \quad (II.10)$$

where, for Munk-Prim flows, the density is related to the velocity by equation (I.4). This equation, expressed in general tensor form, is

$$\rho = \frac{P_0}{RT_0} \left(1 - \frac{g^{ij} V_i V_j}{2 c_p T_0} \right)^{\frac{1}{\gamma-1}} \quad (II.11)$$

One is reminded that P_0 , T_0 , and Ω^i are known variables in the inner loop.

To solve equations (II.8) to (II-10), we introduce the following iterative scheme which is suggested by the work of Martin (ref. 8): ($n = 1, 2, 3, \dots$)

$$\frac{\partial \tilde{F}^1(n)}{\partial x^1} + \frac{\partial \tilde{F}^2(n)}{\partial x^2} + \frac{\partial \tilde{F}^3(n)}{\partial x^3} = 0 \quad (II.12)$$

$$\frac{\partial \tilde{F}^3(n)}{\partial x^2} - \frac{\partial \tilde{F}^2(n)}{\partial x^3} = \frac{\partial F^{3(n-1)}}{\partial x^2} - \frac{\partial F^{2(n-1)}}{\partial x^3} \quad (II.13)$$

$$\frac{\partial \tilde{F}^1(n)}{\partial x^3} - \frac{\partial \tilde{F}^3(n)}{\partial x^1} = \frac{\partial F^{1(n-1)}}{\partial x^3} - \frac{\partial F^{3(n-1)}}{\partial x^1} \quad (II.14)$$

$$\frac{\partial \tilde{F}^{2(n)}}{\partial x^1} - \frac{\partial \tilde{F}^{1(n)}}{\partial x^2} = \frac{\partial F^{2(n-1)}}{\partial x^1} - \frac{\partial F^{1(n-1)}}{\partial x^2} \quad (\text{II.15})$$

$$\frac{\partial \tilde{V}_1^{(n)}}{\partial x^1} + \frac{\partial \tilde{V}_2^{(n)}}{\partial x^2} + \frac{\partial \tilde{V}_3^{(n)}}{\partial x^3} = \frac{\partial V_1^{(n-1)}}{\partial x^1} + \frac{\partial V_2^{(n-1)}}{\partial x^2} + \frac{\partial V_3^{(n-1)}}{\partial x^3} \quad (\text{II.16})$$

$$\frac{\partial \tilde{V}_3^{(n)}}{\partial x^2} - \frac{\partial \tilde{V}_2^{(n)}}{\partial x^3} = \sqrt{g} \, \Omega^1 \quad (\text{II.17})$$

$$\frac{\partial \tilde{V}_1^{(n)}}{\partial x^3} - \frac{\partial \tilde{V}_3^{(n)}}{\partial x^1} = \sqrt{g} \, \Omega^2 \quad (\text{II.18})$$

$$\frac{\partial \tilde{V}_2^{(n)}}{\partial x^1} - \frac{\partial \tilde{V}_1^{(n)}}{\partial x^2} = \sqrt{g} \, \Omega^3 \quad (\text{II.19})$$

Here $F^{1(n-1)}$ and $V_1^{(n-1)}$ are, respectively, the values of F^1 and V_1 at the end of $(n-1)$ -th iteration. $\tilde{F}^{i(n)}$ and $\tilde{V}_i^{(n)}$ are, respectively, the intermediate values of F^1 and V_1 at n -th iteration. The above iteration scheme is motivated by reasons which will be made clear shortly. For now, it suffices to note that these equations uniquely define all of the intermediate variables at n -th iteration if all of the variables at the end of $(n-1)$ -th iteration are known and proper boundary conditions are imposed. This iterative scheme is used solely in a given computation space, therefore, equations (II.12) to (II-19) and any equations to be derived from them shall not be considered as tensor equations. However, in order to economize the presentation of the iterative equations to follow, we shall continue to use tensor notations and Einstein convention with one important exception, i.e., the usual tensor analysis convention concerning the positioning (upper or lower) of indices will be disregarded.

Equations (II.12) to (II-19) do not provide the mechanism for updating the variables without tilda. Six additional equations must be supplied to perform this task. Two of the many possible sets of relationship are given by the equations

$$\text{Scheme 1:} \quad V_1^{(n)} = \tilde{V}_1^{(n)} \quad (\text{II.20})$$

$$F^{1(n)} = \rho^{(n)} \sqrt{g} \, g^{1j} V_j^{(n)} \quad (\text{II.21})$$

Scheme 2:
$$F^i(n) = \tilde{F}^i(n) \quad (II.22)$$

$$v_i^{(n)} = \frac{1}{\rho^{(n-1)} \sqrt{g}} g_{ij} F^j(n) \quad (II.23)$$

where $\rho^{(n)}$ is related to $v_i^{(n)}$ by equation (II.11) for Munk-Prim flow.

If Scheme 1 is used to update the variables without tilda, then $v_i^{(n)}$ and $F^i(n)$ become a function of $\tilde{v}_i^{(n)}$. The tilda variable $\tilde{F}^i(n)$ plays no role in the updating of $v_i^{(n)}$ and $F^i(n)$ and hence only equations (II.16) to (II.19) need to be solved. Conversely, if Scheme 2 is used, then both $F^i(n)$ and $v_i^{(n)}$ become functions of $\tilde{F}^i(n)$ and only equations (II.12) to (II.15) need to be solved. It is noted that the use of Scheme 1, effectively solves equation (II.9) while leaving equation (II.8) unsolved. This fact follows directly from equations (II.17) to (II.20). Conversely, the use of Scheme 2 solves equation (II.8) while leaving equation (II.9) unsolved. For the current solver, Schemes 1 and 2 are used alternatively. In other words, Scheme 1 is used initially and at all subsequent iterations for which n is odd while Scheme 2 is used when n is even. If this iterative procedure converges, the resulting solution must satisfy equations (II.8) to (II.11).

To simplify equations (II.12) to (II.19), we first introduce the variables $f^i(n)$ which are defined by:

$$f^i(n) \stackrel{\text{def.}}{=} \tilde{F}^i(n) - F^i(n-1) \quad (II.24)$$

Equations (II.13) to (II.15) coupled with equation (II.24) imply that

$$\epsilon^{ijk} \frac{\partial f^k(n)}{\partial x^j} = 0 \quad (II.25)$$

As a result, there exists a scalar function $\varphi^{(n)}$ such that

$$f^i(n) = \frac{\partial \varphi^{(n)}}{\partial x^i} \quad (II.26)$$

Combining equations (II.24) and (II.26), one obtains

$$\tilde{F}^i(n) = F^i(n-1) + \frac{\partial \varphi^{(n)}}{\partial x^i} \quad (II.27)$$

Substituting equation (II.27) into equation (II.12), the Poisson's equation for $\varphi^{(n)}$, i.e.,

$$\frac{\partial^2 \varphi^{(n)}}{\partial x^i \partial x^i} = - \frac{\partial F^{(n-1)}}{\partial x^i} \quad (II.28)$$

is obtained. Thus, we have successfully reduced equations (II.12) to (II.15) to a single Poisson's equation (eq. (II.28)). If $\varphi^{(n)}$ is known, $\tilde{F}^{(n)}$ can be calculated using equation (II.27).

Next equations (II.16) to (II.19) are transformed into a set of Poisson equations. We again introduce a correction variable $\hat{f}_i^{(n)}$ which this time is defined as:

$$\hat{f}_i^{(n)} \stackrel{\text{def.}}{=} \tilde{V}_i^{(n)} - V_i^{(n-1)} \quad (II.29)$$

Using equation (II.29), equation (II.16) becomes

$$\frac{\partial \hat{f}_i^{(n)}}{\partial x^i} = 0 \quad (II.30)$$

Thus there is a vector potential $\psi_i^{(n)}$ such that (ref. 15)

$$\hat{f}_i^{(n)} = \epsilon^{ijk} \frac{\partial \psi_k^{(n)}}{\partial x^j} \quad (II.31)$$

and

$$\frac{\partial \psi_i^{(n)}}{\partial x^i} = 0 \quad (II.32)$$

Combining equations (II.29) and (II.31), one obtains

$$\tilde{V}_i^{(n)} = V_i^{(n-1)} + \epsilon^{ijk} \frac{\partial \psi_k^{(n)}}{\partial x^j} \quad (II.33)$$

Substituting equation (II.33) into equations (II.17) to (II.19) and using equation (II.32), we obtain

$$\frac{\partial^2 \psi_i^{(n)}}{\partial x^j \partial x^j} = \epsilon^{ijk} \frac{\partial V_k^{(n-1)}}{\partial x^j} - \sqrt{g} \Omega^i \quad (II.34)$$

Equations (II.16) to (II.19) have thus been reduced to three Poisson's equations (II.34) and a gauge condition (II.32). Equation (II.33) defines $\tilde{v}_i^{(n)}$ in terms of $\psi_i^{(n)}$. At first glance, equations (II.32) and (II.34) give the impression that the three unknowns $\psi_i^{(n)}$'s are overspecified by four independent differential equations. This, however, is incorrect as will be shown.

We first noted that the tensor form of equation (I.9) is

$$\frac{\partial (\sqrt{g} \Omega^i)}{\partial x^i} = 0 \quad (II.35)$$

which coupled with equation (II.34) yields

$$\frac{\partial^2}{\partial x^j \partial x^j} \left(\frac{\partial \psi_i^{(n)}}{\partial x^i} \right) = 0 \quad (II.36)$$

Thus $\left(\frac{\partial \psi_i^{(n)}}{\partial x^i} \right)$ satisfies Laplace's equation if $\psi_i^{(n)}$ satisfies equation (II.34).

If we choose the boundary conditions (B.C.S) for $\psi_i^{(n)}$ such that $\left(\frac{\partial \psi_i^{(n)}}{\partial x^i} \right)$ vanishes at all the boundaries of the computational domain, equation (II.32) is the unique solution of equation (II.36). In other words, the gauge condition (II.32) is satisfied in the entire solution domain if and only if it is satisfied at the boundaries.

Equations (II.16) to (II.19) can be simplified in yet another fashion if a particular solution U_k of equation (II.9) is known. The vector U_k , by definition, is required to satisfy the equation

$$\epsilon^{ijk} \frac{\partial U_k}{\partial x^j} = \sqrt{g} \Omega^i \quad (II.37)$$

If, in addition, we define a variable $\bar{f}_i^{(n)}$ such that

$$\bar{f}_i^{(n)} = \tilde{v}_i^{(n)} - U_i \quad (II.38)$$

Then equations (II.17) to (II.19) and (II.37) imply that the Curl of $\bar{f}_i^{(n)}$ vanishes, i.e.,

$$\epsilon^{ijk} \frac{\partial \bar{f}_k^{(n)}}{\partial x^j} = 0 \quad (II.39)$$

Then, there must exist a scalar $\sigma^{(n)}$ such that

$$\bar{f}_i^{(n)} = \frac{\partial \sigma^{(n)}}{\partial x^i} \quad (II.40)$$

which when combined with equation (II.38), yields

$$\tilde{v}_i^{(n)} = U_i + \frac{\partial \sigma^{(n)}}{\partial x^i} \quad (II.41)$$

Upon substituting this result into equation (II.16) one obtains

$$\frac{\partial^2 \sigma^{(n)}}{\partial x^i \partial x^i} = \frac{\partial}{\partial x^i} \left(v_i^{(n-1)} - U_i \right) \quad (II.42)$$

This time, equations (II.16) to (II.19) have been reduced to a single Poisson's equation (eqs. (II.42) and (II.41)) which updates $\tilde{v}_i^{(n)}$ in terms of U_i and $\sigma^{(n)}$.

Of the two methods presented for solving equations (II.16) to (II.19), the second method has the advantage of solving only one Poisson's equation (eq. (II.42)) instead of three (eq. (II.34)). Its disadvantage is that it requires a particular solution of U_i of equation (II.9) to be known. To circumvent this problem, the following strategy is adopted: Each time through the inner loop, the vector potential method (i.e., the first method discussed) is used to obtain $\tilde{v}_i^{(1)}$. Assuming $U_i = \tilde{v}_i^{(1)}$, the second method is then used to obtain $\tilde{v}_i^{(3)}, \tilde{v}_i^{(5)}, \dots$ at subsequent odd iteration cycles. Since $v_i^{(n)}$ and $F^{i(n)}$ are updated in terms of $\tilde{v}_i^{(n)}$ if n is odd and in terms of $F^{i(n)}$ if n is even, the above strategy combined with the method for updating $\tilde{F}^{i(2)}, \tilde{F}^{i(4)}, \dots$ leads to a complete iterative procedure for solving equations (II.8) and (II.9). This procedure, except for the first iteration cycle, involves only recursively solving two Poisson's equations, i.e., equation (II.28) for even n cycles and equation (II.42) for odd n cycles. The construction of the iteration procedure equations (II.12) to (II.19) made this possible.

The boundary conditions required to solve the Poisson's equations are presented in Appendix B. The stability of this scheme is discussed in Appendix C and shown to be a function of the metric tensor g_{ij} .

The equations which appear in the inner loop will be solved numerically. The divergence, grad and curl are approximated by second order central difference operators in the interior of the computational domain. At the boundaries the normal derivative operator which appears in these expressions is approximated by either a second order forward or backward finite difference operator. The finite difference form of the Laplacian is fixed by the Fast Solver (ref. 16) which we use to solve the Poisson equations.

III - APPLICATIONS TO A SHEAR FLOW IN A TURNING CHANNEL

III.1 Problem Definition and Solution Procedure

In this section, the solution procedure outlined in the previous section is used to compute the developing inviscid rotational flow field in a turning channel (fig. 3). This channel is generated from a parallelepiped (fig. 4) in computational space using the following transformation:

$$e^{\pi \bar{x}^1} = \frac{1}{2} \left(\cosh(\pi x^1) - \cos(\pi x^2) \right) \quad (\text{III.1})$$

$$\cos \frac{\pi \bar{x}^2}{2} = \frac{\sqrt{2} \sinh(\pi x^1/2) \cos(\pi x^2/2)}{\sqrt{\cosh(\pi x^1) - \cos(\pi x^2)}} \quad (\text{III.2})$$

$$\bar{x}^3 = x^3 \quad (\text{III.3})$$

where the coordinates $(\bar{x}^1, \bar{x}^2, \bar{x}^3)$ refer to physical space and (x^1, x^2, x^3) to computational space. The transformation between (\bar{x}^1, \bar{x}^2) and (x^1, x^2) is a conformal transformation defined by

$$Z = (2/\pi) \ln(\sinh(\pi W/2)) \quad (\text{III.4})$$

with $Z = (\bar{x}^1, \bar{x}^2)$ and $W = (x^1, x^2)$. The parameters a, b, c , and d which define the flow boundaries are subjected to the conditions $-\infty < a < b < +\infty$ and $0 < c < d < 1$. The floor and ceiling of a channel are at $x^3 = 0$ and $x^3 = e$, ($0 < e < +\infty$). According to equations (III.1) to (III.3), the values of the metric tensor in computational space is given by

$$g_{ij} = \begin{pmatrix} v & 0 & 0 \\ 0 & v & 0 \\ 0 & 0 & 1 \end{pmatrix} \quad (\text{III.5})$$

where

$$v = \frac{\cosh(\pi x^1) + \cos(\pi x^2)}{\cosh(\pi x^1) - \cos(\pi x^2)} \quad (\text{III.6})$$

Equation (III.5) implies that two orthogonal coordinate lines in computational space remain orthogonal in physical space. Also according to equation (III.5) and (III.6), $g_{ij} \rightarrow \delta_{ij}$ (Kronecker Delta symbol) as $|x^1| \rightarrow +\infty$. Therefore, in a

region where x^1 is sufficiently large, the flow equations, the flow description and the channel geometry as viewed from both computational and physical spaces are identical. We shall assume that both the inlet and exit planes lie in such a region.

The first step in solving a Munk-Prim flow problem, as seen from figure 1, is the specification of the inlet flow conditions. The allowable inlet conditions will be limited to those of a parallel entrance flow. Hence, according to equations (B.1) to (B.3), the inlet conditions are specified by an arbitrary axial velocity profile, an arbitrary temperature profile and a uniform pressure profile. In the current study, the inlet conditions are explicitly given by: (Since $v \sim 1$ at the inlet, these conditions can be given directly in computational space)

$$V^1 = V_C \cdot u(x^3, \delta_V), \quad V^2 = V^3 = 0 \quad (\text{III.7})$$

$$T = T_C \cdot u(x^3, \delta_T) \quad (\text{III.8})$$

$$P = P_C \quad (\text{III.9})$$

Here V_C , T_C , P_C , δ_V , and δ_T are constants and $u(x^3, \delta)$ is defined by

$$u(x^3, \delta) = 1 + \delta \cdot \left(\frac{x^3}{e} - \frac{1}{2} \right) \quad (\text{III.10})$$

where e is the height of the channel. For a fixed value of the constant δ , u is a normalized linear function of x^3 with its maximum variation given by δ , i.e.,

$$\frac{1}{e} \int_0^e u(x^3, \delta) dx^3 = 1 \quad (\text{III.11})$$

and

$$\delta = u(e, \delta) - u(0, \delta) \quad (\text{III.12})$$

As a result of this normalization, the constants V_C and T_C are the average inlet axial velocity and the average inlet temperature. The constants P_C and T_C always can be assigned a value of

$$P_C = T_C = 1 \quad (\text{III.13})$$

by a proper choice of the reference state variables P^* and T^* . The inlet flow conditions can thus be specified solely in terms of V_c , δ_v , and δ_T .

From these conditions, the inlet flow profiles of a substitute flow can be derived using equations (B.4), (B.5), (II.1), (II.3), and (II.4). The inlet profiles of the function τ and μ (see eq. (I.14)) which are consistent with the above inlet flow conditions are given by equation (B.6).

Prior to the start of iteration the substitute flow is initialized so that the density ρ and the contravariant mass flux vector density F^1 satisfy the following conditions:

$$\frac{\partial \rho}{\partial x^1} = 0, \quad \frac{\partial F^1}{\partial x^1} = 0, \quad F^2 = F^3 = 0 \quad (\text{III.14})$$

These equations coupled with the given inlet profiles for ρ and F^1 uniquely determine the initial values of ρ and F^1 within the computational domain. Subsequently, the contravariant velocity field V^1 can be evaluated through the relation: $V^1 = F^1 / (\rho \sqrt{g})$. The flow field so initialized is consistent with the inlet flow conditions, the solid wall boundary conditions (eq. (B.8)) and the continuity equation (eq. (II.8)).

Following the flow initiation, the solver will iterate between the inner and outer loops until the values of P_0 , T_0 , and $\hat{\Omega}$ generated by two consecutive outer loops converge to a preassigned tolerance level. The converged solution to the substitute flow problem is then used to construct the solution to the original problem according to the theory of Section II.1.

The finite difference solutions to the various equations which form the inner and outer loops are constructed using the basic grid shown in figure 5. This grid is channel conforming with uniform spacing in each direction in computational space. This uniformity, however, is lost in physical space.

The stability of the algorithm for solving the transport equations is insured by subdividing each basic grid interval Δx^1 into M equally spaced subintervals. The length of these subintervals, δx^1 , is chosen such that the stability criteria

$$\frac{|V^2|}{V^1} \frac{\delta x^1}{\Delta x^2} < 1 \quad \text{and} \quad \frac{|V^3|}{V^1} \frac{\delta x^1}{\Delta x^3} < 1 \quad (\text{III.15})$$

is satisfied everywhere on the refined grid. In this equation Δx^2 and Δx^3 are, respectively, the lengths of the basic grid intervals in the x^2 and x^3 directions. The refined grid velocity field is obtained by linearly interpolating the basic grid velocity field provided by the inner loop.

III.2 Numerical Results

This subsection will be devoted to assessing the ability of the solver to capture the physics of the development of inviscid secondary flows in a turning channel. In order to perform this assessment, six problems were analyzed. For each problem, the values of the parameters previously defined are tabulated in Table I. In addition, the values of the grid parameters NX1, NX2, and NX3 which define the number of grid intervals in the x^1 , x^2 , and x^3 directions are also tabulated along with the value of NX1S which equals the number of sub-intervals in a grid interval Δx^1 . The value of the parameters c and d were chosen to yield a channel of nearly constant width (approximately equal to $(d-c)$) in physical space. For all six problems the specified inlet flow conditions and channel geometry insure subsonic flow conditions. The inlet Mach number based on V_c and $T_c (=1)$ for the first two cases is 0.0845; for the remaining four problems, its value is 0.4.

The first two problems were constructed to examine the ability of the solver to reproduce the theoretical results of incompressible weak secondary flow theory. For these problems the specified inlet flow conditions lead to the establishment of a homentropic flow. Thus these flows were calculated without the aid of the Munk-Prim substitution principle. For the limiting case of incompressible weak secondary flow, Squire and Winter (ref. 1) derived the expression

$$\xi = 2 \Omega_0 \theta \quad (\text{III.16})$$

for the growth of secondary vorticity along a streamline. In this equation, Ω_0 is the inlet vorticity of the streamline, ξ is the secondary vorticity at any point on the streamline where the local angle of deflection (i.e., the angle between the streamline direction at the inlet and its direction at a point in the channel) is θ . Equation (III.16) implies that, along a streamline, the secondary vorticity increases linearly with θ .

For the chosen channel the values of θ are more or less constant across any cross section. If the imposed inlet flow field is such that all streamlines share a common value of Ω_0 ($\Omega_0 = \delta_v/e$ for the current problems) it is seen that ξ is nearly uniform across any cross section of the channel. The results to be presented for stations A, B, C, D, and E of figures 1 and 2 will be shown to be consistent with these observations. These stations are channel cross sections defined by $x^1 = -1/3$, $x^1 = 0$, $x^1 = 1/3$, $x^1 = 2/3$, and $x^1 = 1$, respectively. In physical space these surfaces are slightly curved. In presenting our results in physical space, we neglect the effect of surface curvature and consider these stations to be flat. This approximation does not introduce any significant errors.

The secondary velocity fields at Stations B and C for the first problem are shown in figure 6. Comparing the magnitude of the displayed velocity vectors to the inlet area averaged velocity of $V_c = 0.1$ (the length scale of the vectors is indicated by a standard vector of magnitude 0.001 at the bottom-right corner of each plot), they are seen to be very small. Thus the theory of Squire and Winter should be applicable to this problem. Both figures show the generated secondary velocity field exhibits a solid body rotational pattern

over most of the cross section, which indicates the secondary vorticity is nearly uniform over each cross section. The only exception occurs in the corner regions where equation (III.16) ceases to be applicable due to excessive streamline curvature.

Furthermore, figure 6 indicates that one may view the line defined by $x^2 = 0.5$ and $x^3 = 0.05$ (according to fig. 4, this line passes through the central grid point at all cross sections) as a streamline since the secondary velocity is nearly zero along this line. At the five points where this approximate streamline intersects Stations A, B, C, D, and E, the values of θ , ξ , and $u/(2\Omega_0\theta)$ for the first two problems are tabulated in Table II. The numerical results are seen to be in excellent agreement with equation (III.16). These results also indicate that, as the flow proceeds further down the channel and the secondary velocity grows larger, nonlinear effects begin to come into play and the agreement between linear theory and numerical results deteriorates.

For the third problem, a significantly larger value of inlet velocity shear was chosen to assess the ability of the solver to capture the physics associated with large secondary flows. Figure 7 shows the secondary velocities that developed at Stations B, C, and E. At Station B, the secondary velocity field is well established, exhibiting the solid body rotation pattern predicted by the linear analysis of Squire and Winter. As the flow proceeds further around the bend, the local secondary velocity field near the four corners grows in magnitude, with a maximum approaching the average inlet velocity $V_c = 0.4733$ (a vector whose magnitude equals the average inlet velocity of 0.4 is depicted at the lower right corner of each figure). This flow structure can no longer be predicted by the linear theory of Squire and Winter. At station E which lies well downstream of the channel bend, the nonlinear behavior grows more evident as two additional vortices appear in the upper-left and lower-right corners. Further down the channel, the secondary flow field becomes more ill defined and begins to take on the appearance of turbulence.

To study other aspects of this homentropic flow, the contours of constant total pressure P_0 at station B, C, and E were computed and are shown in figure 8. Since a surface of constant P_0 is a stream surface (see eq. (I.12)), these illustrations also represent the cross-sectional views of several stream surfaces. For the current problem, the inlet flow conditions vary only in the x^3 -direction. Therefore, the stream surfaces are horizontal at the channel entrance. The contour values of P_0 were chosen to yield contours which coincide with the horizontal grid lines at the entrance to the channel.

As the flow proceeds down the channel, the stream surfaces are rotated by the secondary velocity field to near vertical slightly downstream of Station B. The only exception occurs at the upper-right and lower-left corner regions where they tend to become clustered. This phenomenon can be explained by recalling that every stream surface depicted in figure 8 is swept out by a group of fluid particles which originally passed through a horizontal grid line at the channel entrance. As the flow proceeds down the channel, the fluid particles initially attached to the right (left) side wall will remain attached as long as streamline bifurcation does not take place. In addition these particles are transported toward the top or bottom walls by the secondary velocity field. Since the top and bottom walls are stream surfaces on which P_0 is either a maximum or a minimum (i.e., maximum on the top wall, minimum on the

bottom wall), the fluid particles on the side walls can never reach the top or bottom unless equation (I.12) is violated. They become stagnated when viewed in the cross-sectional plane. This leads to the clustering phenomena depicted in the figure. At Station E, the total pressure contour becomes highly contorted and also shows additional clustering in the upper-left and lower-right corner regions.

The physics of the flow field illustrated in figure 8 is very complex and highly nonlinear. To estimate the accuracy of this solution and, particularly, the impact on solution accuracy of the first order integration scheme for the transport equation, a grid refinement study was undertaken. This study consists of Problems (3), (4), and (5). These three problems represent the solution of the same flow problem (all have identical values of geometric and flow parameters) on three different grids whose cells (in computational space) are geometrically similar. The cell length ratio as well as the subinterval length ratio is 6:4:3. This construction insures that any numerical difference between the solutions to these problems is characterized by a single parameter, i.e., the cell length in any one direction.

Figure 9 shows the contours of constant total pressure computed on the coarse grid at Stations B, C, and E. The contour values of total pressure are again chosen to yield contours which coincide with the horizontal grid lines at the channel entrance. Superimposed on these plots are the corresponding total pressure contours computed using the intermediate and finest grids. At station B (half way around the channel), the results for all three grids are in close agreement. The slight differences one observes are confined to the channel side walls and can be attributed to the inadequate resolution of the clustering of stream surfaces in the corner regions.

As the flow proceeds downstream, the influence of these clustered stream surfaces on the accuracy of the results grows as evident by the contour plots for Station C. These plots show that the results for the coarse and fine grids are only in qualitative agreement, while the results for the intermediate and fine grids still remain in close agreement in the central portion of the channel.

On the side walls, nearly all the contours have been compressed into a single grid interval. The accuracy of the results in this region are therefore questionable and will not be addressed any further in this study. The final comparison is for Station E. The agreement between the three sets of results has suffered additional deterioration, with the results for the intermediate and finest grids now showing only qualitative agreement. One concludes from this study that, except in the corner regions, the results presented in figures 8 are independent of grid size for Stations B and C and can be further improved with additional grid refinement for Station E.

The secondary flows which we have discussed so far have all been generated as a result of an inlet velocity shear. In Problem (6), we examine the secondary flow as generated by a temperature shear. The entering velocity field is uniform, while the inlet temperature and entropy vary in only the x^3 direction. The solution to this general Munk-Prim problem was obtained assuming the substitute flow to be homentropic.

The resulting secondary velocity fields developed at Stations B, C, and E are shown in figure 10. Comparing these results with those on figure 7, it is seen that the secondary velocity fields are very similar except for their sense of rotation. This unexpected result can be explained by recalling that the streamline pattern for Problem (6) is identical to that of the homentropic substitute flow from which it was constructed. This substitute flow has a nega-

tive velocity shear (i.e., axial velocity decreases in the x^3 direction) and a uniform temperature and entropy profile at the channel inlet. These inlet flow conditions with the exception of the sign of the inlet velocity shear are very similar to those for Problem (3). This accounts for their close resemblance. Furthermore, examination of the contours of constant total pressure (not shown) further corroborated the close resemblance of these two problems.

The flow problems discussed thus far have either been solved without the direct use of the Munk-Prim substitution principle (Problems (1) to (5)) or solved assuming a homentropic substitute flow (Problem (6)). They could have been just as easily solved assuming a homenergetic substitute flow. Numerical results based on this alternative formulation for all six problems verified this contention. In fact, the graphs (either the secondary velocity fields or the constant total contours) generated by these two approaches were indistinguishable. This result, along with the successful computation of Problem (6), demonstrates the reliability of the Munk-Prim substitution principle as a tool for steady inviscid flow computation.

CONCLUSIONS

The current algorithm represents a new procedure for solving inviscid subsonic 3-D rotational flows. The convergence for the algorithm is shown to be dependent on the value of the matrix tensor in computational space. Results obtained using this algorithm show that it can accurately predict the behavior of weak secondary flows. Furthermore, the results of a grid refinement study indicate the algorithm is sufficiently accurate to capture the physics of the evolving strong shear flows.

Finally, this work clearly shows that the use of the Munk-Prim substitution principle can substantially reduce the computational effort in solving any 3-D inviscid steady rotational flow problem.

APPENDIX A

Basic Theorems of the Outer Loop

In the current study, the outer loop solves for the vorticity field $\vec{\Omega}$ which satisfies the equations

$$\vec{V} \times \vec{\Omega} = \vec{\nabla} h_0 - T \vec{\nabla} S \quad (\text{A.1})$$

and

$$\vec{\nabla} \cdot \vec{\Omega} = 0 \quad (\text{A.2})$$

Here, \vec{V} , h_0 , T , and S are assumed to be known flow variables with h_0 and S satisfying the equations

$$\vec{V} \cdot \vec{\nabla} h_0 = 0 \quad (\text{A.3})$$

and

$$\vec{V} \cdot \vec{\nabla} S = 0 \quad (\text{A.4})$$

Given the above conditions, we establish the following theorems:

Theorem 1: Assuming $\vec{V} \neq 0$ throughout the region of interest and defining $\vec{e}_v = \frac{\vec{V}}{|\vec{V}|}$ then a solution $\vec{\Omega}$ of equations (A.1) and (A.2) is uniquely defined if the streamwise vorticity $(\vec{\Omega} \cdot \vec{e}_v)$ is specified at the inlet surface.

Proof: Let $\vec{\Omega}'$ and $\vec{\Omega}''$ be two solutions of equations (A.1) and (A.2) with $\vec{\Omega}' \cdot \vec{e}_v = \vec{\Omega}'' \cdot \vec{e}_v$ at the inlet surface. If we define $\delta\vec{\Omega} = \vec{\Omega}'' - \vec{\Omega}'$, then one has

$$\vec{V} \times \delta\vec{\Omega} = 0 \quad (\text{A.5})$$

$$\vec{\nabla} \cdot \delta\vec{\Omega} = 0 \quad (\text{A.6})$$

and, at the inlet surface,

$$\delta\vec{\Omega} \cdot \vec{e}_v = 0 \quad (\text{A.7})$$

Since $\vec{V} \neq 0$, from equation (A.5), one concludes that

$$\delta\vec{\Omega} = \sigma\vec{V} \quad (\text{A.8})$$

where σ is a scalar function. Equations (A.6) to (A-8) imply that

$$\vec{V} \cdot \vec{\nabla}\sigma + (\vec{\nabla} \cdot \vec{V})\sigma = 0 \quad \text{universally} \quad (\text{A.9})$$

and

$$\sigma = 0 \quad \text{at the inlet surface.} \quad (\text{A.10})$$

From equations (A.9) and (A.10) and the assumption $\vec{V} \neq 0$, we conclude that $\sigma = 0$ universally (ref. 17). As a result, $\delta\vec{\Omega} = \sigma\vec{V} = 0$ universally. Thus $\vec{\Omega}' = \vec{\Omega}''$ Q.E.D.

Theorem 2: Assuming $\vec{V} \neq 0$ and either $\vec{\nabla}h \neq 0$ or $\vec{\nabla}S \neq 0$ throughout the region of interest, then for any solution $\vec{\Omega}$ of equations (A.1) and (A.2), there exist infinitely many pairs of functions τ and μ (referred to as the Clebsch potentials associated with $\vec{\Omega}$) such that

$$\vec{\Omega} = \vec{\nabla}h_0 \times \vec{\nabla}\tau + \vec{\nabla}S \times \vec{\nabla}\mu \quad (\text{A.11})$$

$$\vec{V} \cdot \vec{\nabla}\tau = 1 \quad (\text{A.12})$$

and

$$\vec{V} \cdot \vec{\nabla}\mu = -T \quad (\text{A.13})$$

Conversely, for any τ and μ which satisfy equations (A.12) and (A.13), equation (A.11) defines a solution $\vec{\Omega}$ of equations (A.1) and (A.2).

Proof: With the help of equations (A.3), (A.4), (A.12), and (A.13), the second part of this theorem can be proved by directly substituting equation (A.11) into equations (A.1) and (A.2). To prove the first part, first we assume that $\vec{\nabla}h_0 \neq 0$. For any solution $\vec{\Omega}$ of equations (A.1) and (A.2), one introduces a vector field $\vec{\Omega}'$ such that

$$\vec{\Omega}' = \vec{\Omega} - \vec{\nabla}S \times \vec{\nabla}\mu \quad (\text{A.14})$$

Here μ is any function which satisfies equation (A.13). Equations (A.1), (A.2), (A.4), (A.13), and (A.14) imply that

$$\vec{V} \times \vec{\Omega}' = \vec{V} h_0 \quad (\text{A.15})$$

and

$$\vec{V} \cdot \vec{\Omega}' = 0 \quad (\text{A.16})$$

As a result of equation (A.15), one has

$$\vec{\Omega}' \cdot \vec{V} h_0 = 0 \quad (\text{A.17})$$

Equation (A.17) states that h_0 is conserved along any vortex line of $\vec{\Omega}'$. Using equations (A.16) and (A.17), it is shown in reference 18 that there is a scalar function τ such that

$$\vec{\Omega}' = \vec{V} h_0 \times \vec{V} \tau \quad (\text{A.18})$$

provided that $\vec{V} h_0 \neq 0$. Substituting equations (A.18) into (A.15) and using equation (A.3), one obtains equation (A.12) as the condition τ must satisfy. Equation (A.11) follows directly from equations (A.14) and (A.18). Since there are infinitely many choices for μ which satisfies equation (A.13), it is easy to see that there are infinitely many pairs of Clebsch potentials associated with an $\vec{\Omega}$ which satisfies equations (A.1) and (A.2).

If $\vec{V} h_0 = 0$, but $\vec{V} S \neq 0$, a similar proof can be constructed to show that the first part of Theorem 2 is still valid Q.E.D. The above theorem indicates that there are infinitely many pairs of Clebsch potential associated with an $\vec{\Omega}$ which satisfies equations (A.1) and (A.2). The relationship among these Clebsch potentials is established by Theorem 3.

Theorem 3: If τ and μ are a pair of Clebsch potentials associated with an $\vec{\Omega}$ which satisfies equations (A.1) and (A.2), then in a region in which $\vec{V} h_0 \times \vec{V} S \neq 0$, τ' and μ' form another pair of Clebsch potentials associated with the same $\vec{\Omega}$ if and only if there is a function $\varphi(h_0, S)$ such that

$$\tau' = \tau + \frac{\partial \varphi(h_0, S)}{\partial h_0} \quad (\text{A.19})$$

and

$$\mu' = \mu + \frac{\partial \varphi(h_0, S)}{\partial S} \quad (\text{A.20})$$

Proof: By directly substituting equations (A.19) and (A.20) into equations (A.11) to (A.13) and using equations (A.3) and (A.4), it can be shown that (τ', μ') and (τ, μ) are indeed associated with the same $\vec{\Omega}$ if they are related by equations (A.19) and (A.20). To show the "only if" part of this theorem, first we define

$$\delta\tau = \tau' - \tau \quad \text{and} \quad \delta\mu = \mu' - \mu \quad (\text{A.21})$$

Since, by assumption, both (τ', μ') and (τ, μ) are associated with the same $\vec{\Omega}$, equations (A.11) to (A.13) and (A.21) imply that

$$\vec{\nabla} h_0 \times \vec{\nabla} \delta\tau + \vec{\nabla} S \times \vec{\nabla} \delta\mu = 0 \quad (\text{A.22})$$

$$\vec{\nabla} \cdot \vec{\nabla} \delta\tau = 0 \quad (\text{A.23})$$

and

$$\vec{\nabla} \cdot \vec{\nabla} \delta\mu = 0 \quad (\text{A.24})$$

Using equation (A.22), one has

$$\vec{\nabla} S \cdot \vec{\nabla} h_0 \times \vec{\nabla} \delta\tau = 0 \quad (\text{A.25})$$

and

$$\vec{\nabla} h_0 \cdot \vec{\nabla} S \times \vec{\nabla} \delta\mu = 0 \quad (\text{A.26})$$

Equations (A.25) and (A.26) used in conjunction with the assumption that $\vec{\nabla} h_0 \times \vec{\nabla} S \neq 0$ imply that (ref. 19)

$$\delta\tau = f_1(h_0, S) \quad \text{and} \quad \delta\mu = f_2(h_0, S) \quad (\text{A.27})$$

Here f_1 and f_2 are two arbitrary functions of h_0 and S .

Substituting equations (A.27) into equation (A.22) and again invoking the assumption $\vec{\nabla} h_0 \times \vec{\nabla} S \neq 0$ yields

$$\frac{\partial f_1}{\partial S} = \frac{\partial f_2}{\partial h_0} \quad (\text{A.28})$$

As a result of equation (A.28), there exists a function $\varphi(h_0, S)$ that

$$\delta\tau = f_1(h_0, S) = \frac{\partial\varphi(h_0, S)}{\partial h_0} \quad (A.29)$$

$$\delta\mu = f_2(h_0, S) = \frac{\partial\varphi(h_0, S)}{\partial S} \quad (A.30)$$

$\delta\tau$ and $\delta\mu$ as given by equations (A.29) and (A.30) automatically satisfy equations (A.23) and (A.24) if equations (A.3) and (A.4) are taken into account. Equations (A.19) and (A.20) follow directly from equations (A.21), (A.29), and (A.30) Q.E.D. Since $\vec{\nabla}h_0 \times \vec{\nabla}S = 0$ for both homentropic and homenergetic flows,

Theorem 3 cannot be applied to these flows. Therefore the following theorems are given:

Theorem 4: In a region in which $\vec{\nabla}S = 0$ and $\vec{\nabla}h_0 \neq 0$, the function μ introduced in Theorem 2 need not be specified (see eq. (A.11)). If τ is a Clebsch potential associated with an $\vec{\Omega}$ which satisfies equations (A.1) and (A.2), then τ' is another Clebsch potential associated with the same $\vec{\Omega}$ if and only if there is a function $\gamma(h_0)$ such that

$$\tau' = \tau + \gamma(h_0) \quad (A.31)$$

Theorem 5: In a region in which $\vec{\nabla}h_0 = 0$ and $\vec{\nabla}S \neq 0$, the function τ introduced in Theorem 2 need not be specified. If μ is a Clebsch potential associated with an $\vec{\Omega}$ which satisfies equations (A.1) and (A.2), then μ' is another Clebsch potential associated with the same $\vec{\Omega}$ if and only if there is a function $\theta(S)$ such that

$$\mu' = \mu + \theta(S) \quad (A.32)$$

Theorems 4 and 5 can be proved using the same techniques employed in the Proof of Theorem 3. The details will not be presented.

APPENDIX B

Inlet Flow Conditions, Outflow Conditions, and Boundary Conditions

In this appendix, we restrict the analysis to flows which enter the curved channel described in Section III with parallel streamlines. Such flows have inlet conditions described by the following equations:

$$v^1 = r(x^2, x^3), \quad v^2 = v^3 = 0 \quad (B.1)$$

$$P = P_c \quad (B.2)$$

and

$$T = q(x^2, x^3) \quad (B.3)$$

where P_c is a constant and r, q are arbitrary functions of x^2 and x^3 . (As noted in Section III, far upstream and downstream of the channel bend, the values of the metric tensor and thus the forms of fluid dynamic equations are identical in computational and physical space. As a result, equations (B.1) to (B.3) are valid in both spaces.) Using equations (B.1) to (B.3), it can be shown that, at the inlet

$$T_o = q + \frac{r^2}{2C_p} \quad (B.4)$$

$$P_o = P_c \left(1 + \frac{r^2}{2C_p \cdot q} \right)^{\frac{\gamma}{\gamma-1}} \quad (B.5)$$

With the help of equations (II.1), (II.3), and (II.4), equations (B.1), (B.4), and (B.5) can be used to establish the inlet conditions for the substitute flows.

Since the streamlines of the incoming flow are parallel, the inlet streamwise vorticity Ω^1 must vanish. From equation (II.1), the inlet streamwise vorticity $\Omega^{1'}$ of the corresponding substitute flow must also vanish. According to equation (I.19), a choice for the inlet profile of τ' and μ' which yields $\Omega^{1'} = 0$ at the inlet is:

$$\tau' = \mu' = 0 \quad (B.6)$$

With the inlet profiles of τ' and μ' established, the solution of their respective transport equation is uniquely defined.

The construction of the appropriate inlet boundary conditions (B.C.S.) for $\varphi^{(n)}$, $\psi_1^{(n)}$, and $\sigma^{(n)}$ is based on the assumption that the inlet flow condi-

tions do not vary during the course of iteration. As a result, the iterative increments $\hat{f}^{1(n)}$, $f_1^{(n)}$, and $\bar{f}_1^{(n)}$ must satisfy the conditions: ($n = 1, 2, \dots$)

$$f^{1(n)} = \hat{f}_1^{(n)} = \bar{f}_1^{(n)} = 0 \quad (x^1 = a) \quad (B.7)$$

A choice of the inlet B.C.S. for $\varphi^{(n)}$, $\psi_i^{(n)}$, and $\sigma^{(n)}$ which is consistent with both the above condition and the gauge condition (II.32) is given in the first column of Table III.

At the solid walls of the channel, we require the velocity component normal to the walls to vanish. This requirement may be expressed in the tensor form

$$V_i n^i = 0 \quad (B.8)$$

where V_i and n^i are, respectively, the covariant velocity vector and the contravariant normal vector at any point on the wall. For the numerical example treated in Section III, the solid walls are located at $x^2 = c$, $x^2 = d$, $x^3 = 0$, and $x^3 = e$ (See fig. 4). From equations (B.8), (II.10), and the fact that $g_{ij} = 0$ if $i \neq j$, the boundary conditions at these walls become

$$V_2 = F^2 = 0 \quad \text{at} \quad x^2 = c \quad \text{or} \quad x^2 = d \quad (B.9)$$

$$V_3 = F^3 = 0 \quad \text{at} \quad x^3 = 0 \quad \text{or} \quad x^3 = e \quad (B.10)$$

If we initialize the iteration procedure with a flow field which is consistent with the above conditions, the iterative increments $f^{1(n)}$, $\hat{f}_1^{(n)}$, and $\bar{f}_1^{(n)}$ ($i = 2, 3$) must satisfy the following conditions: ($n = 1, 2, \dots$)

$$f^{2(n)} = \hat{f}_2^{(n)} = \bar{f}_2^{(n)} = 0 \quad \text{at} \quad x^2 = c \quad \text{or} \quad x^2 = d \quad (B.11)$$

$$f^{3(n)} = \hat{f}_3^{(n)} = \bar{f}_3^{(n)} = 0 \quad \text{at} \quad x^3 = 0 \quad \text{or} \quad x^3 = e \quad (B.12)$$

A choice of the B.C.S. for $\varphi^{(n)}$, $\psi_i^{(n)}$, and $\sigma^{(n)}$ at the solid walls which is consistent with both the above conditions and the gauge condition (II.32) is given in the second and third columns of Table III.

At the channel exit, a fixed set of outflow conditions are directly imposed on the substitute flow in computational space. The initial outflow con-

ditions are identical to the initial inlet flow conditions. The exit B.C.S. for $\phi^{(n)}$, $\psi_1^{(n)}$, and $\sigma^{(n)}$ are given in the fourth column of Table III. These B.C.S. insure the gauge condition equation (II.32) is satisfied, and in the limit of incompressible flow yield

$$\frac{\partial V_1^{(n)}}{\partial x^1} = 0 \quad (B.13)$$

for any n .

APPENDIX C

Inner Loop Stability Analysis

In this appendix, the stability of the inner loop iteration is analyzed assuming the density ρ is held fixed. This assumption would be compatible with a solver in which the density is updated only in the outer loop.

As in Section III, we shall use tensor notations in this study to economize the mathematical expressions even though they may not be tensor expressions. We assume that $V_i^{(n)}$ and $F^{1(n)}$ are updated by equations (II.20) and (II.21) if $n = 1, 3, 5, \dots$ and updated by equations (II.22) and (II.23) if $n = 2, 4, 6, \dots$. Furthermore, we assume that $\tilde{F}^i(n)$ and $\tilde{V}_i^{(n)}$ are solved with the help of equations (II.27) and (II.33). ($\tilde{V}_i^{(n)}$ could also be solved using equation (II.41) if $n = 3, 5, 7, \dots$. This alternative approach, however, does not alter the resulting convergence criterion equation (C.11)). The above assumptions coupled with equations (II.12), (II.17) to (II.19), (II.28), and (II.34) imply that, for $n = 2, 4, 6, \dots$

$$\frac{\partial \psi_1^{(n+1)}}{\partial x^j \partial x^j} = \epsilon^{ijk} \frac{\partial}{\partial x^j} \left(\frac{g_{kl}}{\rho \sqrt{g}} \frac{\partial \varphi^{(n)}}{\partial x^l} \right) \quad (C.1)$$

and

$$\frac{\partial^2 \varphi^{(n+2)}}{\partial x^i \partial x^i} = - \frac{\partial}{\partial x^i} \left(\rho \sqrt{g} g^{ij} \epsilon^{jkl} \frac{\partial \psi_l^{(n+1)}}{\partial x^k} \right) \quad (C.2)$$

To study the stability of the inner loop iterations, we shall assume that

$$\varphi^{(n)} \rightarrow \varphi^{(\infty)} \quad \text{and} \quad \psi_1^{(n+1)} \rightarrow \psi_1^{(\infty)} \quad \text{as} \quad n \rightarrow +\infty \quad (C.3)$$

Furthermore, it is assumed that ($n = 2, 4, 6, \dots$)

$$\varphi^{(n)} - \varphi^{(\infty)} = \text{Re} \left(\varphi^{(n)} e^{IP_j x^j} \right) \quad (C.4)$$

and

$$\psi_1^{(n+1)} - \psi_1^{(\infty)} = \text{Re} \left(\psi_1^{(n+1)} e^{IP_j x^j} \right) \quad (C.5)$$

where P_j is the wave propagation vector, $\underline{\psi}^{(n)}$ and $\underline{\psi}_i^{(n+1)}$ the perturbation amplitudes, Re = the real part of the quantity in the parenthesis, and

$$I = \sqrt{-I}.$$

This assumption is realistic only if the magnitude of P_i is large (i.e., we deal with only high wave number disturbance) compared with the characteristic wave numbers of the spatial variations of ρ , g , g_{ij} , and g^{ij} . As a result, ρ , g^{ij} , and g_{ij} are considered as constants in equations (C.1) and (C.2). A direct substitution of equations (C.3) to (C.5) into equations (C.1) and (C.2) yields

$$\underline{\psi}_i^{(n+1)} = \frac{1}{\rho \sqrt{g}} \epsilon^{ijk} g_{kl} \tilde{p}_j \tilde{p}_l \underline{\psi}^{(n)} \quad (\text{C.6})$$

and

$$\underline{\psi}^{(n+2)} = -\rho \sqrt{g} g^{ij} \epsilon_{jkl} \tilde{p}_i \tilde{p}_k \underline{\psi}_l^{(n+1)} \quad (\text{C.7})$$

Here \tilde{p}_i are the directional cosines of the vector P_i , i.e.,

$$\tilde{p}_i \stackrel{\text{def.}}{=} \frac{P_i}{\sqrt{P_j P_j}} \quad (\text{C.8})$$

and thus

$$\tilde{p}_i \tilde{p}_i = (\tilde{p}_1)^2 + (\tilde{p}_2)^2 + (\tilde{p}_3)^2 = 1 \quad (\text{C.9})$$

Note that equations (C.5) and (C.6) are consistent with the gauge condition equation (II.32). If one substitutes equation (C.6) into equation (C.7), the final result is

$$\underline{\psi}^{(n+2)} = \left[1 - \left(g^{ij} \tilde{p}_i \tilde{p}_j \right) \left(g_{kl} \tilde{p}_k \tilde{p}_l \right) \right] \underline{\psi}^{(n)} \quad (\text{C.10})$$

Since $n = 2, 4, 6, \dots$, equation (C.10) implies that the stability of the inner loop iterations requires that $\left| 1 - \left(g^{ij} \tilde{p}_i \tilde{p}_j \right) \left(g_{kl} \tilde{p}_k \tilde{p}_l \right) \right| \leq 1$ or equivalently

$$2 \geq \left(g^{ij} \tilde{p}_i \tilde{p}_j \right) \left(g_{kl} \tilde{p}_k \tilde{p}_l \right) \geq 0 \quad (C.11)$$

for any \tilde{p}_i which satisfies equation (C.8).

To solve equation (C.11), we note that the matrices formed by g^{ij} and g_{kl} are positive definite hermitian matrices and are the inverse of each other. Assuming that λ_1, λ_2 , and λ_3 ($\lambda_1 \geq \lambda_2 \geq \lambda_3 > 0$) are the eigenvalues of g_{kl} , it can be shown that (ref. 20):

$$\frac{(\lambda_1 + \lambda_3)^2}{4\lambda_1\lambda_3} \geq \left(g^{ij} \tilde{p}_i \tilde{p}_j \right) \left(g_{kl} \tilde{p}_k \tilde{p}_l \right) \geq 1 \quad (C.12)$$

It should be noted that $(\lambda_1 + \lambda_3)^2 / (4\lambda_1\lambda_3)$ and 1 are, respectively, the least upper bound and the greatest lower bound of $\left(g^{ij} \tilde{p}_i \tilde{p}_j \right) \left(g_{kl} \tilde{p}_k \tilde{p}_l \right)$ if the domain of \tilde{p}_i includes all \tilde{p}_i which satisfy equation (C.9). Combining equation (C.11) with equation (C.12), one obtains

$$6 \geq \frac{\lambda_1}{\lambda_3} + \frac{\lambda_3}{\lambda_1} \quad (C.13)$$

For the current numerical study, g_{kl} is given by equations (III.5) and (III.6). As a result, equation (C.13) reduces to

$$\frac{1}{\sqrt{2}} \geq \frac{\cos(\pi x^2)}{\cosh(\pi x)} \geq -\frac{1}{\sqrt{2}} \quad (C.14)$$

The validity of the above stability condition has been verified by numerical experiments.

REFERENCES

1. Squire, H. B.; and Winter, K. G.: The Secondary Flow in a Cascade of Airfoils in a Non-Uniform Stream. *J. Aerosp. Sci.*, vol. 18, 1951, pp. 271-277.
2. Hawthorne, W. R.: Secondary Circulation in Fluid Flow. *Proc. R. Soc., London, Ser. A*, vol. 206, 1951, pp. 374-387.
3. Hawthorne, W. R.: The Growth of Secondary Circulation in Frictionless Flow. *Proc. Cambridge Philos. Soc.*, vol. 51, no. 4, Oct. 1955, pp. 737-743.
4. Lakshminarayana, B.; and Horlock, J. H.: Generalized Expressions for Secondary Vorticity Using Intrinsic Coordinates. *J. Fluid Mech.*, vol. 59, pt. 1, 1973, pp. 97-115.
5. Pratap, V. S.; and Spalding, D. B.: Fluid Flow and Heat Transfer in Three-Dimensional Duct Flows. *Int. J. Heat Mass Transfer*, vol. 19, 1976, pp. 1183-1188.
6. Briley, W. R.; and McDonald, H.: Analysis and Computation of Viscous Subsonic Primary and Secondary Flows. *AIAA Paper 79-1453*, 1979.
7. Abdallah, S.; and Hamed, A.: An Inviscid Solution for the Secondary Flow in Curved Ducts. *AIAA Paper 80-1116*, June 1980.
8. Martin, E. D.: A Split-Recoupled-Semidirect Computational Technique Applied to Transonic Flow over Lifting Airfoils. *AIAA Paper 78-11*, Jan. 1978.
9. Moore, J.; and Moore, J. G.: A Calculation Procedure for Three-Dimensional, Viscous, Compressible Duct Flow. Part II - Stagnation Pressure Losses in a Rectangular Elbow. *ASME Paper 79-WA/FE-5*, Dec. 1979.
10. Hamed, A.; and Abdallah, S.: A New Approach for Solving the Vorticity and Continuity Equations in Turbomachinery Ducts. *AIAA Paper 79-0046*, Jan. 1979.
11. Munk, M.; and Prim, R. C.: On the Multiplicity of Steady Gas Flows Having the Same Streamline Pattern. *Proc. Nat. Acad. Sci. U.S.A.*, vol. 33, no. 5, 1947, pp. 137-141.
12. Vazsonyi, A.: On Rotational Gas Flows. *Quart. Appl. Math.*, vol. 3, 1945, pp. 29-37..
13. Hartree, D. R.: *Numerical Analysis*. 2nd ed., University Press, Oxford, 1958.
14. Abramowitz, M.; and Stegun, I. A.: *Handbook of Mathematical Functions with Formulas, Graphs, and Mathematical Tables*, National Bureau of Standards. 1956, p. 882.

15. Morse, P. M.; and Feshbach, H.: *Methods of Theoretical Physics*. McGraw-Hill, 1953, Part 1, p. 53.
16. Adams, J.; Swarztrauber, P.; and Sweet, R.: FISHPAK: Efficient FORTRAN Subprograms for the Solution of Separable Elliptic Partial Differential Equations, Version 3. National Center for Atmospheric Research, Boulder, Colo., 1978.
17. Courant, R.; and Hilbert, D.: *Methods of Mathematical Physics*. Vol. 2, Interscience, 1962, Chap. 2.
18. Lamb, H.: *Hydrodynamics*. 6th Ed., Cambridge University Press, 1932, p. 248.
19. Phillips, H. B.: *Vector Analysis*. John Wiley & Sons, 1933, p. 41.
20. Greub, W., and Rheinboldt, W., "On a Generalization of An Inequality of L. V. Kantorovich," American Mathematical Society Proceedings, Vol. 11, 1959, pp. 407-415.

TABLE 1. - FLOW PROBLEMS AND THEIR DEFINING PARAMETERS

Problem	Geometric parameters					Flow parameters				Grid parameters			
	a	b	c	d	e	γ	V_c	δ_v	δ_T	NX1	NX2	NX3	NX1S
No. 1 ^a	-2.0	2.0	0.45	0.55	0.1	1.4	0.1	0.01	0.0	72	6	6	12
No. 2 ^a	↓	↓	↓	↓	↓	↓	0.1	0.02	↓	72	6	6	↓
No. 3 ^b	↓	↓	↓	↓	↓	↓	0.4733	0.2	↓	144	12	12	↓
No. 4 ^b	↓	↓	↓	↓	↓	↓	0.4733	0.2	↓	108	9	9	↓
No. 5 ^b	↓	↓	↓	↓	↓	↓	0.4733	0.2	↓	72	6	6	↓
No. 6 ^c	↓	↓	↓	↓	↓	↓	0.4733	0.0	0.3	144	12	12	↓

^aHomentropic and linear.^bHomentropic and nonlinear.^cInhomentropic, inhomenergetic, and nonlinear.

TABLE 2. - NUMERICAL COMPARISONS WITH EQUATION (III.16)

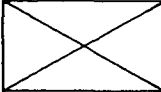

	Station	A	B	C	D	E
	θ (radian)	0.6750	1.5708	2.4667	2.8965	3.0552
Problem No. 1 ($\alpha_0 = 0.1$)	ξ	0.013432	0.031329	0.049137	0.057498	0.060317
	$\xi/(2\alpha_0\theta)$	0.99498	0.99722	0.99604	0.99254	0.98712
Problem No. 2 ($\alpha_0 = 0.2$)	ξ	0.026856	0.062547	0.097549	0.11294	0.11708
	$\xi/(2\alpha_0\theta)$	0.99470	0.99546	0.98870	0.97475	0.95806

TABLE 3. - THE BOUNDARY CONDITIONS FOR $\varphi^{(n)}$, $\sigma^{(n)}$, and $\psi_1^{(n)}$

	$x^1 = a$	$x^2 = c$ $x^2 = d$	$x^3 = 0$ $x^3 = e$	$x^1 = b$
$\varphi^{(n)}$	$\frac{\partial \varphi^{(n)}}{\partial x^1} = 0$	$\frac{\partial \varphi^{(n)}}{\partial x^2} = 0$	$\frac{\partial \varphi^{(n)}}{\partial x^3} = 0$	$\varphi^{(n)} = 0$
$\sigma^{(n)}$	$\frac{\partial \sigma^{(n)}}{\partial x^1} = 0$	$\frac{\partial \sigma^{(n)}}{\partial x^2} = 0$	$\frac{\partial \sigma^{(n)}}{\partial x^3} = 0$	$\sigma^{(n)} = 0$
$\psi_1^{(n)}$	$\frac{\partial \psi_1^{(n)}}{\partial x^1} = 0$	$\psi_1^{(n)} = 0$	$\psi_1^{(n)} = 0$	$\frac{\partial \psi_1^{(n)}}{\partial x^1} = -\left(\frac{\partial \psi_2^{(n)}}{\partial x^2} + \frac{\partial \psi_3^{(n)}}{\partial x^3}\right)$
$\psi_2^{(n)}$	$\psi_2^{(n)} = 0$	$\frac{\partial \psi_2^{(n)}}{\partial x^2} = 0$	$\psi_2^{(n)} = 0$	$\frac{\partial \psi_2^{(n)}}{\partial x^1} = 0$
$\psi_3^{(n)}$	$\psi_3^{(n)} = 0$	$\psi_3^{(n)} = 0$	$\frac{\partial \psi_3^{(n)}}{\partial x^3} = 0$	$\frac{\partial \psi_3^{(n)}}{\partial x^1} = 0$

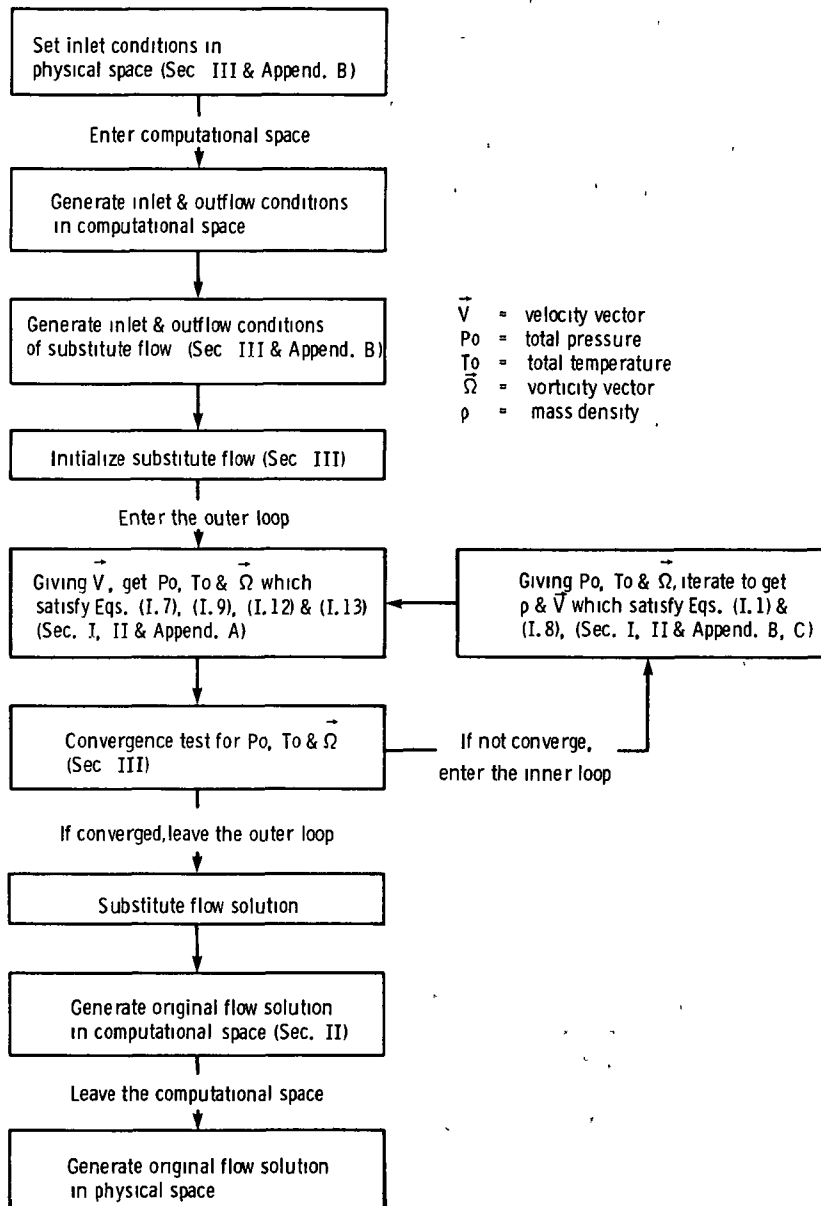


Figure 1. - The flow chart for munk-prim flow solver.

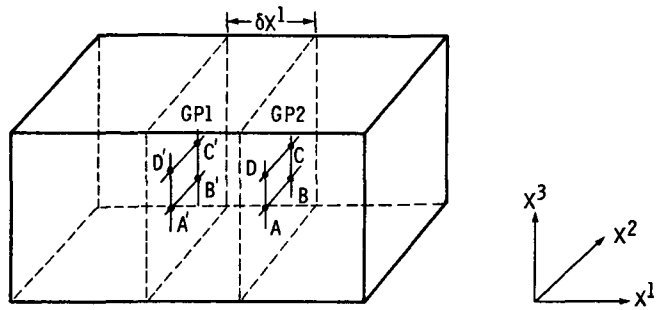
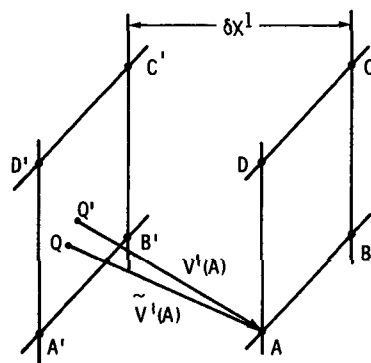


Figure 2 (a). - Two adjacent grid planes GP1 and GP2



$$\tilde{V}^1(A) = 1/2 (V^1(A) + V^1(Q'))$$

Figure 2 (b) - The marching method for transport equations.

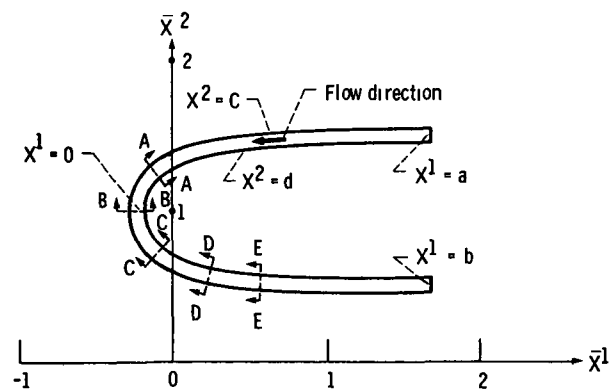


Figure 3. - The physical space (\bar{x}^3 is suppressed).

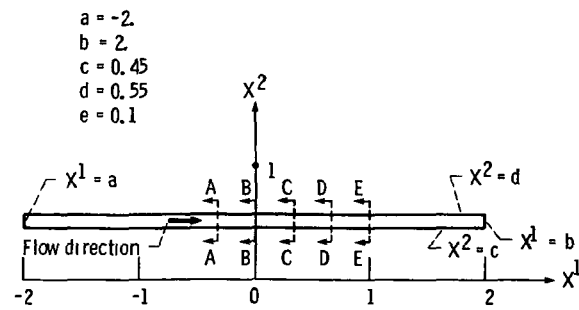


Figure 4 - The computational space (X^3 is suppressed).

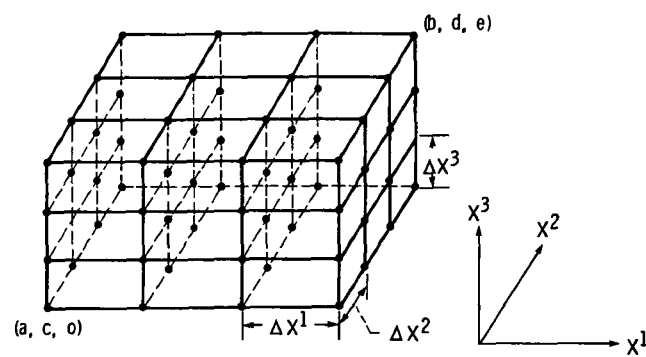


Figure 5. - A $4 \times 4 \times 4$ basic mesh in computational space.

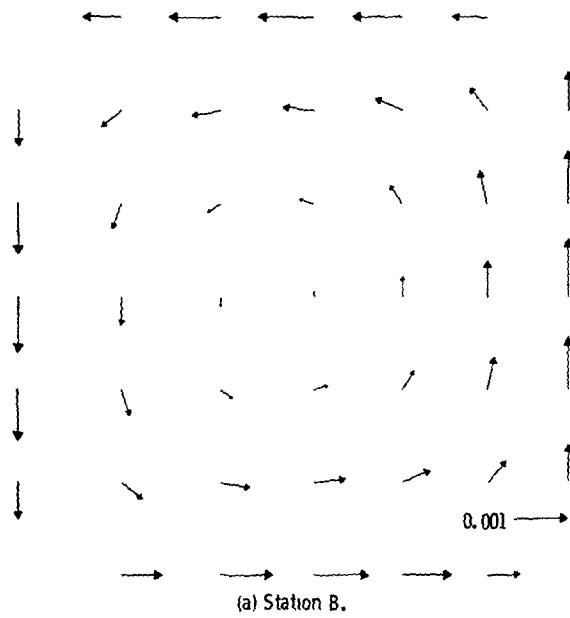


Figure 6. - Secondary velocity field for problem (1).

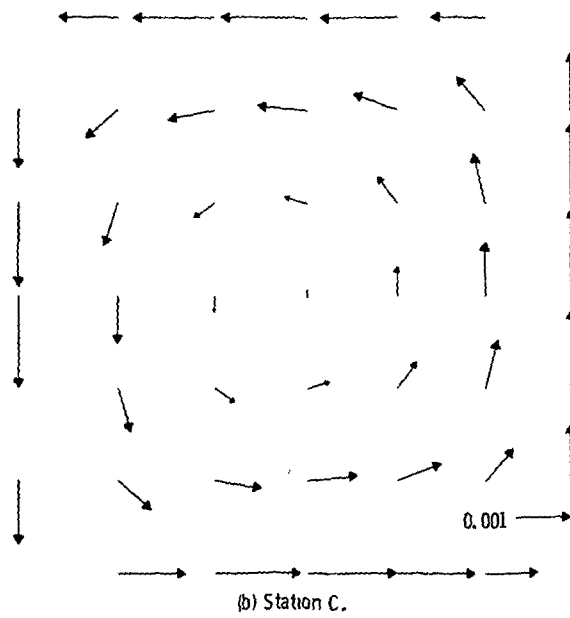
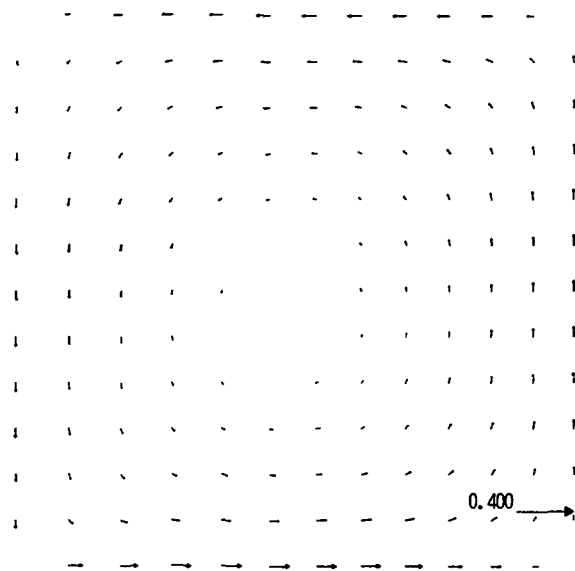
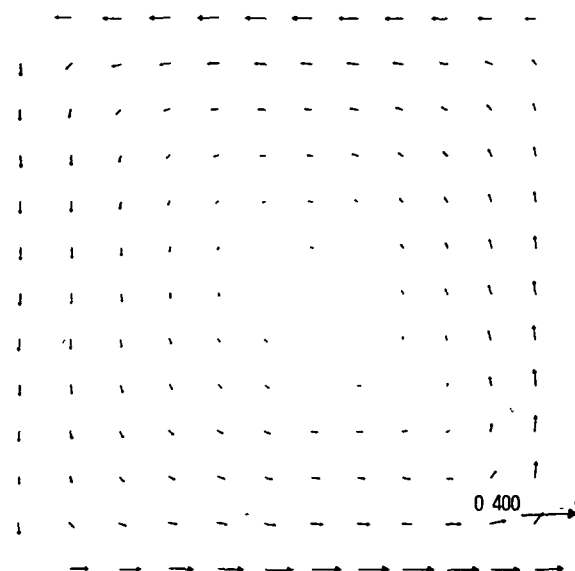


Figure 6. - Concluded.



(a) Station B.

Figure 7. - Secondary velocity field for problem (3).



(b) Station C.

Figure 7. - Continued.

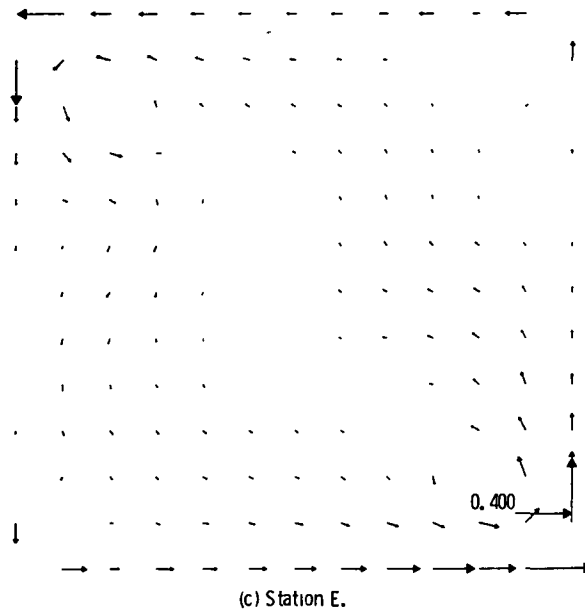


Figure 7. - Concluded.

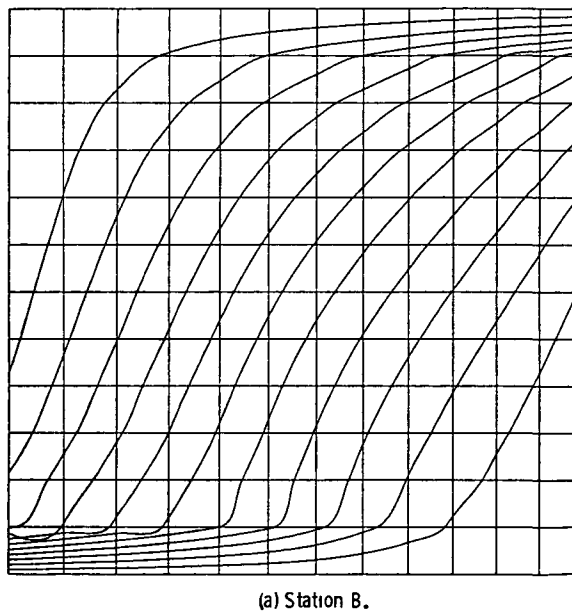
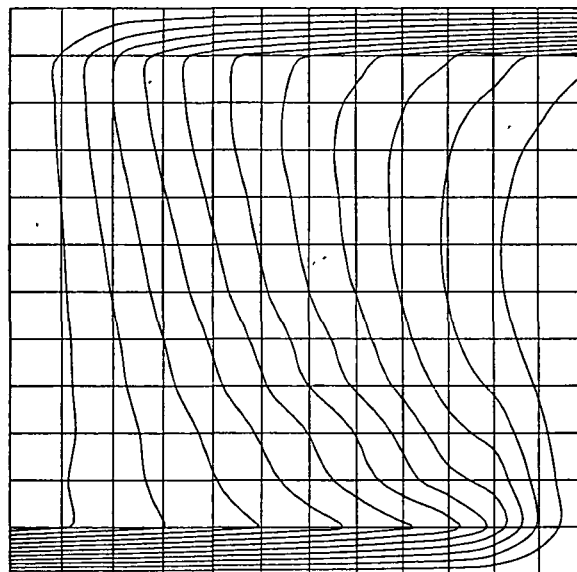
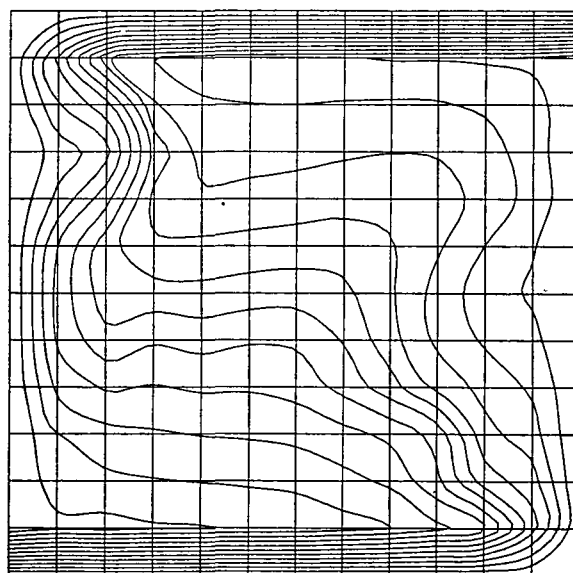


Figure 8. - Total pressure contours for problem (3).



(b) Station C.

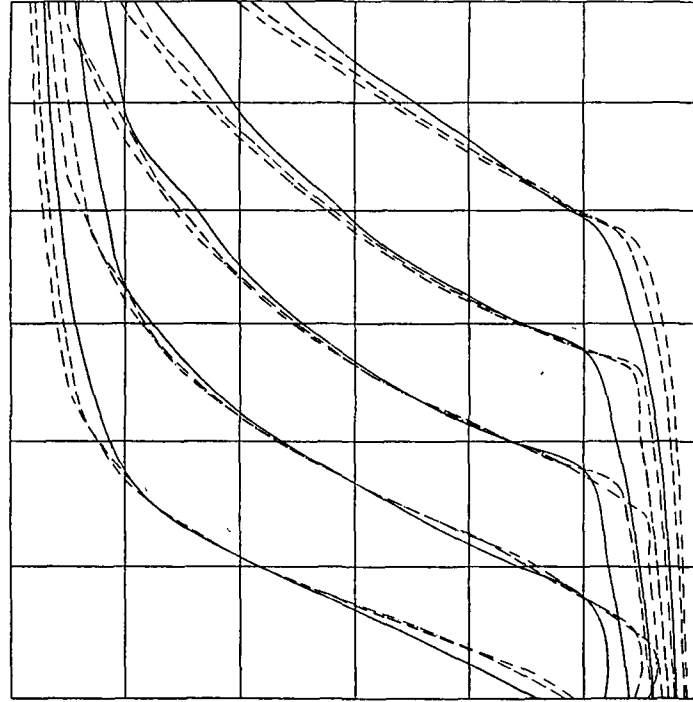
Figure 8. - Continued.



(c) Station E.

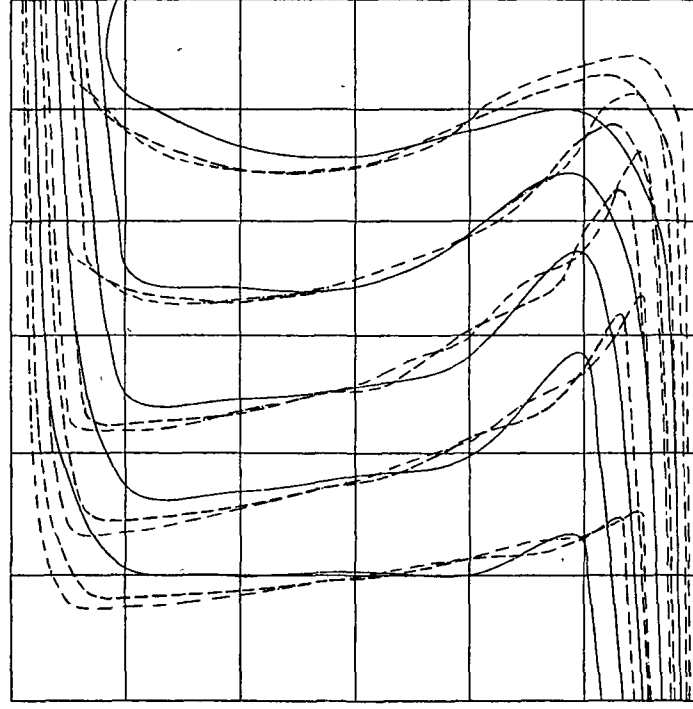
Figure 8. - Concluded.

--- Problem (3)
 --- Problem (4)
 --- Problem (5)



(a) Station B.

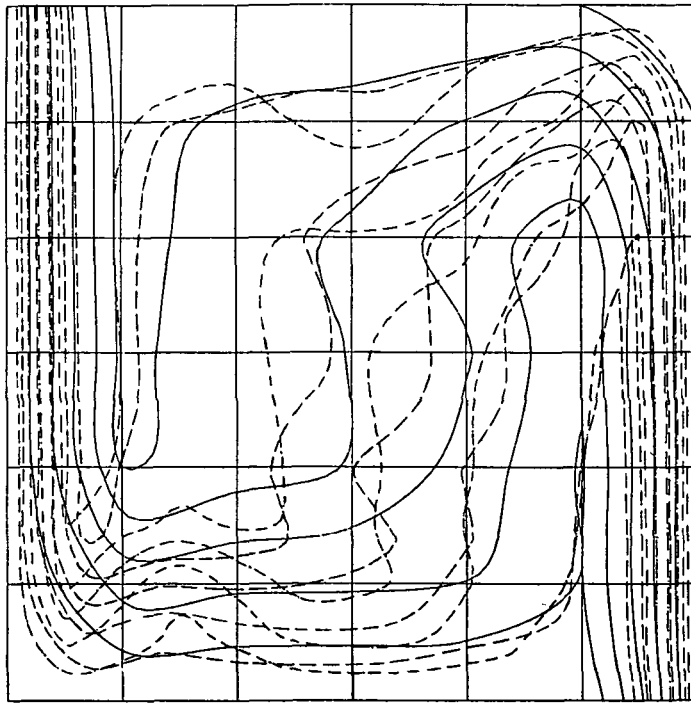
--- Problem (3)
 --- Problem (4)
 --- Problem (5)



(b) Station C.

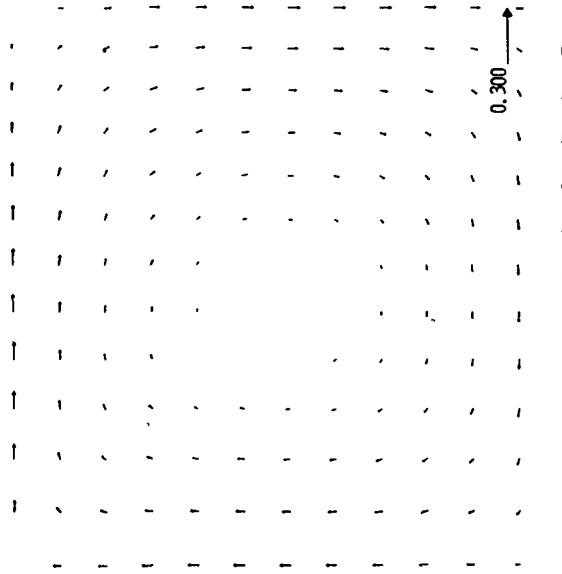
Figure 9. - Continued.

--- Problem (3)
 --- Problem (4)
 --- Problem (5)



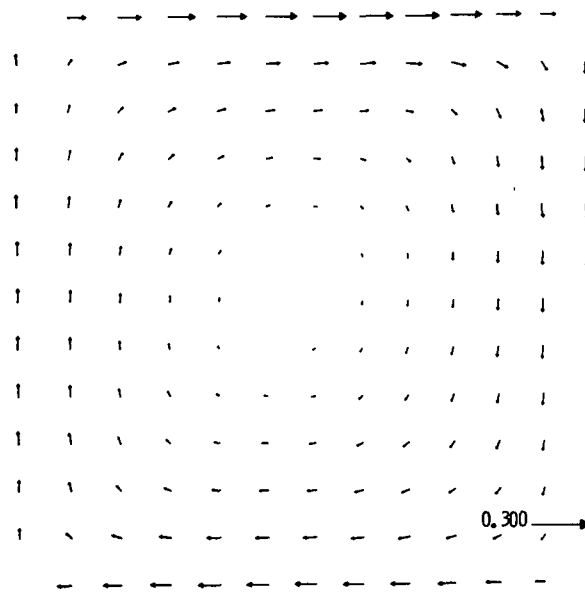
(c) Station E.

Figure 9. - Concluded.



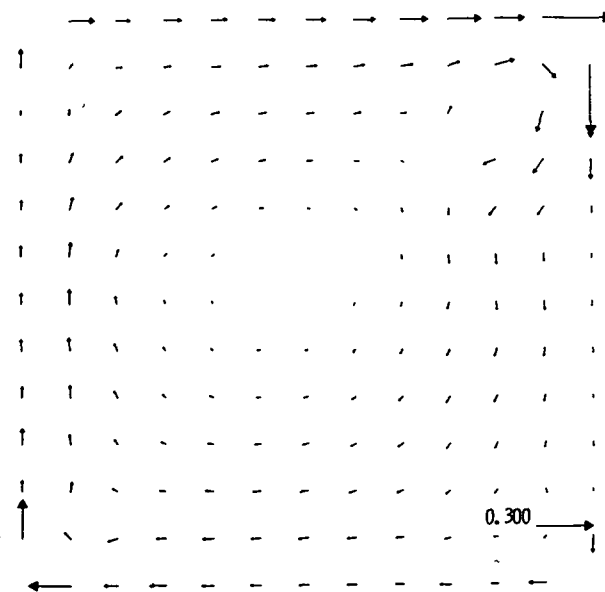
(a) Station B.

Figure 10 - Secondary velocity field for problem (4).



(b) Station C.

Figure 10 - Continued.



(c) Station E.

Figure 10 - Concluded.

1 Report No NASA TM-83314	2 Government Accession No	3 Recipient's Catalog No	
4 Title and Subtitle A SEMI-DIRECT SOLVER FOR COMPRESSIBLE THREE-DIMENSIONAL ROTATIONAL FLOW		5 Report Date May 1983	
		6 Performing Organization Code 505-31-01	
7. Author(s) Sin-Chung Chang and John J. Adameczyk		8 Performing Organization Report No E-1556	
		10 Work Unit No	
9. Performing Organization Name and Address National Aeronautics and Space Administration Lewis Research Center Cleveland, Ohio 44135		11 Contract or Grant No	
		13 Type of Report and Period Covered Technical Memorandum	
12 Sponsoring Agency Name and Address National Aeronautics and Space Administration Washington, D. C. 20546		14 Sponsoring Agency Code	
15 Supplementary Notes			
16 Abstract An iterative procedure is presented for solving steady inviscid 3-D subsonic rotational flow problems. The procedure combines concepts from classical secondary flow theory with an extension to 3-D of a novel semi-direct Cauchy-Riemann solver. It is developed for generalized coordinates and can be exercised using standard finite difference procedures. The stability criterion of the iterative procedure is discussed along with its ability to capture the evolution of inviscid secondary flow in a turning channel.			
17 Key Words (Suggested by Author(s)) 3-D rotational flows		18 Distribution Statement Unclassified - unlimited STAR Category 02	
19. Security Classif (of this report) Unclassified	20 Security Classif (of this page) Unclassified	21. No of Pages	22 Price*

National Aeronautics and
Space Administration

Washington, D.C.
20546

Official Business

Penalty for Private Use, \$300

SPECIAL FOURTH CLASS MAIL
BOOK



Postage and Fees Paid
National Aeronautics and
Space Administration
NASA-451

NASA

POSTMASTER ·

If Undeliverable (Section 154
Postal Manual) Do Not Return

24 JUN 10 JUL 1984